Available online at www.sciencedirect.com

ScienceDirect

Applied Energy 00 (2022) 1–36

Applied Energy

Data-Driven Identification of Lithium-ion Batteries: A Nonlinear Equivalent Circuit Model with Diffusion Dynamics

Chuanxin Fan[a,*], Kieran O'Regan[b,c], Liuying Li[a,c], Matthew D. Higgins[a], Emma Kendrick[b,c], Widanalage D. Widanage[a,c]

[a] *WMG, University of Warwick, Coventry, CV4 7AL, United Kingdom*
[b] *School of Metallurgy and Materials, University of Birmingham, Edgbaston, Birmingham, BT15 2TT, United Kingdom*
[c] *The Faraday Institution, Quad One, Becquerel Avenue, Harwell Campus, Didcot, OX11 0RA, United Kingdom*

Abstract

An accurate battery model is essential for battery management system (BMS) applications. However, existing models either don't describe battery physics or are too computationally intensive for practical applications. This paper presents a non-linear equivalent circuit model with diffusion dynamics (NLECM-diff) which phenomenologically describes the main electrochemical behaviours, such as ohmic, charge-transfer kinetics, and solid-phase diffusion. A multisine approach is applied to identify the elements for high frequency dynamics, as well as a distributed SoC dependent diffusion model block is optimised to account for long time dynamics. The model identification procedure is conducted on a three-electrode experimental cell, such that NLECM-diff models are developed for each electrode to then obtain the full cell voltage. Results imply that the NLECM-diff reduces the voltage root mean square error (RMSE) by 49.6% compared to a conventional ECM in the long duration discharge and has comparable accuracy to a parameterised SPMe in the NEDC driving cycle. Additionally, the variation of diffusion-related characteristics of the negative electrode under different currents is determined as the primary reason of the battery models' large low-SoC-range error. Furthermore, the diffusion process is determined as the dominant voltage loss contributor in the long duration discharge and the ohmic voltage loss is identified as the dominant dynamic under NEDC driving profile.

Keywords: Battery modelling, System identification, Multisine excitation, Surface state of charge, Non-linear equivalent circuit model

1. Introduction

Lithium-ion batteries (LIB) have gained increasing attention as storage for electric energy in a variety of fields, including portable devices, electric vehicles (EVs), and power grids, due to their high energy density and long cycle life [1]. In larger systems, a battery management system (BMS) is responsible for assessing various battery state variables, such as state-of-charge (SoC), state-of-power (SoP), and state-of-health (SoH), to determine the energy,

*Corresponding author
Email address: Chuanxin.Fan@warwick.ac.uk (Chuanxin Fan)

Nomenclature

$\bar{v}_0$	Measured over-potential	H_{exc}	Excited harmonics
$\bar{z}$	Average state of charge	$H_{supp,even}$	Even suppressed harmonics
η_D	Voltage loss caused by diffusion	$H_{supp,odd}$	Odd suppressed harmonics
η_R	Non-linear voltage loss caused by charge-transfer kinetics	i_0	Exchange current
		K	Highest harmonic number
τ	Time constant	N	Number of samples
$\tilde{u}$	Scaled multisine signal	P	Total periods of multisine signal
φ	Phase of signal	Q	Capacity-related parameter
A	Amplitude of signal	R	Molar gas constant
c_1	Linear coefficient of sigmoid function	R_0	Internal ohmic resistance
c_2	Non-linear coefficient of sigmoid function	R_p	Polarisation resistance
C_p	Polarisation capacitance	T	Temperature
F	Faraday's constant	U	Open circuit voltage
f_s	Sampling frequency	v_l	Modelled over-potential

power capability, and 'health', respectively [2–4]. Also, efficient optimization and safe charging strategies to prolong battery service life are the BMS's responsibility [5–9].

State-estimation and optimization algorithms are based on mathematical models, to higher or lower degrees of complexity, of a battery. By interpreting the electrochemical behaviours in the electrodes and electrolyte, physics-based electrochemical models have been proposed to describe the lithium-ion battery over the past few years. Newman *et al.* firstly designed the porous electrode theory to describe models for lithium-ion cells, now known as the Doyle-Fuller-Newman (DFN) model [10]. Non-linear electrochemical processes, such as mass transport and charge-transfer kinetics, are considered in this model, which enables the DFN model to maintain a high degree of accuracy under a majority of operational cases. Furthermore, the separate electrode and electrolyte dynamics offer the ability to couple parasitic reactions for ageing and capacity fade modelling [11, 12]. However, due to the partial differential equations (PDEs) utilized in the porous electrode theory, the practical application of the DFN model is restricted by the heavy calculation load for solving PDEs. In addition, a total of around 35 parameters are required in the DFN model and some of these parameters must be identified by complicated physical chemical experiments, which increases its difficulty of parametrization [13]. To reduce the complexity of the electrochemical model, several simplifications of the DFN model have been proposed in recent years. In Ref. [14], the authors reviewed the simplified electrochemical models such as the porous electrode model with the polynomial approximation (PP) and the initial single particle model (SPM). The key idea of the SPM is that the solid phase of each electrode is assumed as a uniform single spherical particle and concentration changes in the electrolyte are neglected. The results show that the computational time

and cost of simplified model are significantly less than those of the rigorous DFN model. However, due to the lack of Li^+ concentration distribution and the potential distribution of the electrolyte phase, the model accuracy cannot be maintained for large current inputs. In addition, an improved SPM, named as SPMe, was derived in Ref. [15], which comprises of the solid phase and the electrolyte phase dynamics and requires a total of 29 parameters. The additional terms, which represent ohmic potential drop due to electrolyte conductivity and the electrolyte concentration overpotential, allows this model to retain accuracy for large input currents. Despite the fact that these simplified models require less calculation cost than the DFN model, microprocessors in a practical BMS cannot run the electrochemical models in a high resolution as resolving concentration and potential gradients in the solid phase commonly requires finite difference or finite element numerical schemes to solve PDEs [16]. In recent years, to support on-broad applications, model order reduction techniques, such as residue grouping [17, 18], balanced truncation [19], Padé approximation [20], have been used to further reduce the order of the SPM, SPMe or DFN model while retaining the appropriate level of accuracy. However, the SPM, SPMe or reduced order model is essentially a physics-based electrochemical model, and determining their physical parameters during model development (e.g. electrode thicknesses, porosities, etc.), still pose as an obstacle for practical onboard applications.

A different category of battery models, termed as conventional linear equivalent circuit models (ECMs), utilizes a number of simple electrical circuit components, such as resistors, capacitor and inductors, to imitate the current and voltage relationship of a lithium-ion battery. To identify such models, the nature of battery's dynamics must be extracted from data collected during specially designed characterization tests. For example, traditional ECMs are commonly identified by Hybrid Pulse Power Characterization (HPPC) [21], Pulse Charge (PC) and Pulse Discharge (PD) tests [22, 23], and multisine tests [24, 25]. Unlike the parameterization for physical models which requires related background and physical chemical experimental skills, data-driven identification approaches do not require any prespecified knowledge of the battery system. The model's structure and parameters are determined using measured input current and output voltage signal, which is advantageous for battery researchers and engineers. Taking advantage of the lower computational load and easier parameterization than electrochemical models, the ECM is widely applied in battery management systems for model-based state-estimation methods [26–28]. However, there are several limitations. A ECM is a phenomenological description and cannot directly associate an electrical circuit component to a certain battery physical phenomena, which limits the detailed insight of lithium-ion battery behaviours. ECMs are also linear parameter varying models. The model parameters (ohmic resistance, time constants), can vary with SoC and temperature, but for a given SoC and temperature, the current to voltage relationship is linear. In addition, ECMs are typically at most 2nd order (2 RC pairs) and usually parameterised via HPPC pulses. The voltage losses an ECM model accounts for are the ohmic loss (via the series resistor) and the polarisation loss (via the 2 RC branches). However, the RC branches in an ECM represent the short time constant ($\sim$ 10s of seconds) polarisation but do not reflect the polarisation due to diffusion dynamics - long time constant ($\sim$ 1000s of seconds).

In recent years, to improve model accuracy by accounting for battery non-linearity explicitly, a non-linear equivalent circuit model (NLECM) composed of a distinct linear and non-linear block has been developed using frequency

domain approaches. Rather than extrapolating parameters at various SOC levels, the NLECM explicitly interprets battery nonlinearity by nonlinear function to improve model accuracy. Widanage *et al.* designed pulse-multisine signals as the identification excitation to capture the battery linear and non-linear dynamic behaviour in real-world driving [29]. Furthermore, based on the experimental data obtained via the pulse-multisine input, a NLECM for a lithium-ion battery was developed which exhibits lower root mean square error (RMSE) and peak error than a conventional linear ECM [24]. However, the accuracy of the NLECM over the entire state-of-charge (SoC) range was not investigated in [24] and the energy type battery used in the study only exhibits weak non-linearity in the room temperature case. Authors in [30] developed and parametrized a Hammerstein-Wiener structure non-linear model for all-solid-state batteries. However, only the low frequency range ($f < 1$ Hz) for capturing the diffusion dynamic was considered in this work. An advantage with a NLECM is that the physics phenomena of batteries can be related to its linear and non-linear parts, which may provide valuable information that a conventional linear ECM cannot contain [24]. For instance, in a NLECM, the linear block represents the electrical behaviour on the internal ohmic resistance and the non-linear block describes the non-linear dependence of the voltage on the current due to charge-transfer kinetics. Meanwhile, since the NLECM can also keep calculation load to a minimum and a low parameter identification effort, it is qualified as a suitable candidate for practical BMS applications [31].

On contrary to electrochemical models, the effect of solid-phase diffusion process in a lithium-ion battery is seldom considered in the ECM modelling approach, which leads to poor accuracy at long time (low frequency) operational cases [32]. To the best of the authors' knowledge, only a handful of literatures have taken into account the diffusion process in ECM modelling, and the interpretation of the diffusion process is thought to improve model precision. Wang *et al.* proposed to incorporate the effect of diffusion as a resistance into an one resistor-capacitor (RC) pair model to improve the power prediction [32]. However, the diffusion resistance is assumed as an additional conventional resistance in the RC pair and is not considered during the ECM parameter estimation. To enhance the model accuracy at low SoC range, Ouyang *et al.* proposed an extended equivalent circuit model (EECM) to represent the effect of diffusion process to terminal voltage by the SoC difference in electrode particles which is calculated from two RC branches [33]. Unfortunately, the nonlinear charge-transfer kinetic has not been explicitly interpreted by the two RC branches and the number of EECM parameters that needs to be estimated increases from six to ten for addressing the diffusion effect only. In Ref.[34], the authors incorporated three distinct diffusion models, such as using a common Resistor-Capacitor (RC) circuit element or using a diffusion equation in an idealized particle with or without the parameter indicating the open circuit voltage curve dependency on SoC, into conventional linear equivalent circuit models, respectively. The results show that the diffusion models improved voltage prediction compared to an ECM not including any diffusion. But the performance evaluation of ECM with diffusion was only compared with convention ECMs under dynamic current loads, rather than including the physical-based electrochemical models, and the performance during long time operation is not taken into account. In Ref.[35], a fractional-order model is proposed to interpret dynamics in a lithium-ion battery including an electrochemical impedance spectroscopy (EIS) sub-model for mid-high frequency dynamic, however, transformation of EIS model elements into the time domain for onboard

applications is not trivial. Thus, a high computational efficiency and readily parameterisable model, which also can describe battery physical meaning and nonlinearity, is required for the real-world application.

1.1. Contribution of the paper

In this paper, we propose an advanced non-linear equivalent circuit model with diffusion dynamics, termed as NLECM-diff, established by a data-driven system identification approach, which can explicitly interpret the essential physical phenomena in a lithium-ion battery such as ohmic, charge-transfer kinetics, and diffusion dynamics. In the NLECM-diff model, a non-linear equivalent circuit model (NLECM) encompassing a linear ECM for ohmic impedance with polarization and a non-linear sigmoid function for charge-transfer kinetics is identified by applying a multisine-based non-linear characterization method using a three-electrode cell where the electrodes have been extracted from the 21700 cylindrical LG M50 cell [36]. In addition, for improving model accuracy, especially at low SOC range, a simplified SoC-dependent diffusion model solved by using a Chebyshev pseudo-spectral method is incorporated into the NLECM-diff model to interpret the contribution of diffusion dynamics to the terminal voltage on the cell level. The NLECM-diff model is fully parameterizable with voltage and current data from both multisine excitation and constant current discharge experiments, rather than the need to perform specific complicated experiments to get geometric, transport and kinetic parameters. Additionally, taking advantage of the instrumented cell with a stable reference electrode, NLECM-diff models are also developed for each electrode to estimate the internal potential variable. The accuracy of the NLECM-diff models are compared with the single particle model with electrolyte dynamic (SPMe) and validation experiments including a long time discharge charge profile and a dynamic driving cycle. The origin of low-SoC-range error for battery models as well as the dominant voltage loss caused by certain electrochemical processes contributing to terminal voltage are unequivocally determined by applying the NLECM-diff models.

1.2. Organization of the paper

In Section 2 of this paper, the multisine excitation signal designed and experiment setup for the model identification are described. Section 3 explains the modelling approach of the non-linear equivalent circuit battery model with diffusion dynamics, including a frequency domain identification method for the NLECM and a parametrization process for the diffusion model. The advantage of the proposed model over the conventional NLECM is also evaluated and analysed in Section 3. The model validation and comparison to electrochemical models are discussed in detail in Section 4. Section 5 presents the conclusion and recommended future work.

2. Multisine excitation signal design and experiment setup

2.1. Odd random phase multisine signal design

In this study, an odd random phase multisine signal was designed as an excitation current signal for model identification. Compared to traditional HPPC tests, the multisine signal has been applied as an advanced characterisation

method that can capture and separate the dominant linear response, nonlinear distortion (nonlinearity), and noise distortion of a lithium-ion battery [36, 37]. Such that, not only the traditional linear model, but also the nonlinear function for interpreting the battery's nonlinear voltage-current relationship can be built in accordance with the characterisation data. Additionally, the multisine signal has a wider bandwidth, a greater amplitude, and a shorter test duration than the conventional HPPC test [29]. As a periodic broadband signal (a signal that repeats), the multisine is designed by the superposition of multiple sinusoidal waves with customized frequencies, which provides flexibility in the design of its amplitude spectrum and harmonic content [38]. The expression of a general multisine excitation signal is as Eq. (1).

$$u(n) = \sum_{k=1}^{K} A_k \sin\left(2\pi n k f_s/N + \varphi_k\right) \qquad n = 0, ..., N-1 \tag{1}$$

Where N is the number of samples per period, K denotes the highest harmonic number of the signal, f_s is the sampling frequency, A_k is the amplitude and φ_k is the phase of the kth harmonic. The N of a multisine can be flexibly determined and the frequency resolution is equal to $f_0 = f_s/N$. According to the Shannon sampling theorem, the highest possible harmonic K is then less than or equal to $N/2$. Thus, the highest possible frequency of the multisine signal can be equal to the product $f_0 \times K$ and should span the characteristic frequency range for the battery experiment. To ensure that there is no net change in SoC upon the application of the multisine signal during the characterization tests, the DC frequency, which is $k = 0$ harmonic, is suppressed for obtaining a zero-mean current signal.

When a multisine signal is applied to a nonlinear system (battery included), some energy injected at the excited current harmonics in the excitation signal will be transferred and observed at the other harmonic positions in the output voltage spectrum, which indicates the system nonlinearities [39, 40]. To characterize the nonlinearity of a battery for modelling the NLECM non-linear block, the harmonic content f_k, harmonic phases φ_k, and amplitude spectrum A_k are the key components which require to be determined in the signal design procedure. The multisine signal is designed as an odd multisine and suppresses all even harmonics within the bandwidth considered. However, not all odd harmonics are excited, an odd harmonic in each group of three consecutive odd harmonics (e.g. 1,3, 5 or 7,9,11) is randomly selected and suppressed. All the suppressed even and odd harmonics act as non-linear detection harmonics is the output voltage spectrum. The set of excited harmonics is denoted as H_{exc} and the sets of suppressed harmonics are termed as $H_{supp,odd}$ and $H_{supp,even}$ with respect to the odd and even harmonics. The motivation of suppressing harmonics is that the suppressed odd and even harmonics can be utilized for detecting the odd and the even order nonlinearities, respectively [41]. The phases of the excited harmonics can be set to obtain different amplitude distributions to excite the dynamics around a certain operating point [42, 43]. In this study they are randomly sampled from a uniform distribution between 0 and 2π (hence the terminology of odd-random phase multisine). In addition, the amplitudes A_k are identical to unit across all the excited harmonics (a flat spectrum), and the root-mean square (rms) value of the designed multisine signal can be scaled in the time domain to the desired

value M for a specific amplitude. Let $\widetilde{u}(n)$ be the scaled multisine and is related to $u(n)$ as follows:

$$\tilde{u}(n) = M\frac{u(n)}{||\mathbf{u}||_\infty} \tag{2}$$

In Eq. (2), M is the desired maximum magnitude of the random-phase multisine signal and $\mathbf{u} = [u(0), ..., u(N-1)]$.

In this study, the bandwidth of the odd random phase multisine signal was set as 10 Hz to include the low and partial mid characteristic frequency ranges, such that the dominant nonlinearities caused by both diffusion and charge-transfer kinetics behaviour can be characterized [36]. Given that the sampling frequency f_s of the hardware is 50 Hz, the number of sample per period N is set to $N = 5000$ giving a signal periods of 100 s. The frequency resolution is therefore $f_0 = 1/100$ Hz. A total 334 odd harmonics out of all $K = N/2 = 2500$ harmonics were excited giving $H_{exc} = \{1, 5, 7, 9, 13, 15, 21, 23, ..., 999\}$ from 10 mHz to 10 Hz. To improve the robustness of the characterization results, the periodic input multisine signal $u(n)$ is repeated $P = 10$ times per SoC and thus the total duration will be $T_{total} = P \times 100\,\text{s} = 1000\,\text{s}$ at any given SoC. In addition, the designed random phase φ_n of the excited harmonics is a uniformly distributed random variable between 0 to 2π. Finally, the factor M was set at 11.5 to scale the multisine signal magnitude to $1C$ of the three-electrode configuration experimental cells that will be introduced later in order to characterise any battery nonlinearity .

In this work, the designed multisine tests are conducted at five SoC points 10%, 30%, 50%, 70%, and 90%, for the NLECM-diff identification. Fig.1 shows the performance of the designed multisine current signal recorded by hardware when the battery is at 50% SoC and 25 °C. The measured and designed multisine input current in the time domain have been shown in Fig.1(a) and the frequency spectrum of the measured current calculated by discrete Fourier transform in Fig.1(b). Note that, due the feature of random phase in the multisine signal, the maximum current amplitude may be larger than the desired RMS magnitude. In this work, the peak value of the current signal reaches to 40.4 mA which is 3.5 times larger than 1 C-rate,11.5 mA. Given that the limitation of hardware signal generator in some cases, the signal optimization technique might need to be considered [38]. However, it's out of scope in this study. Furthermore, as can be seen in Fig.1(b), each excited sinusoidal wave (blue crosses with 7 dB) is larger than the nonlinearity levels at around −65 dB and the noise level at around −80 dB. Fig.1(c) shows the current error between measured and designed multisine signal. The large magnitude gap between the spectrum levels and the small order magnitude (10^{-4}) of the current error indicate that the hardware platform was at a good condition which only introduces neglectable environment and measurement noise. As multisine is inherently made as a zero-mean signal, the SoC variation in one period was extremely small (less than 0.01%), as shown in Fig.1(d), such that the OCV change can be neglected during the multisine test.

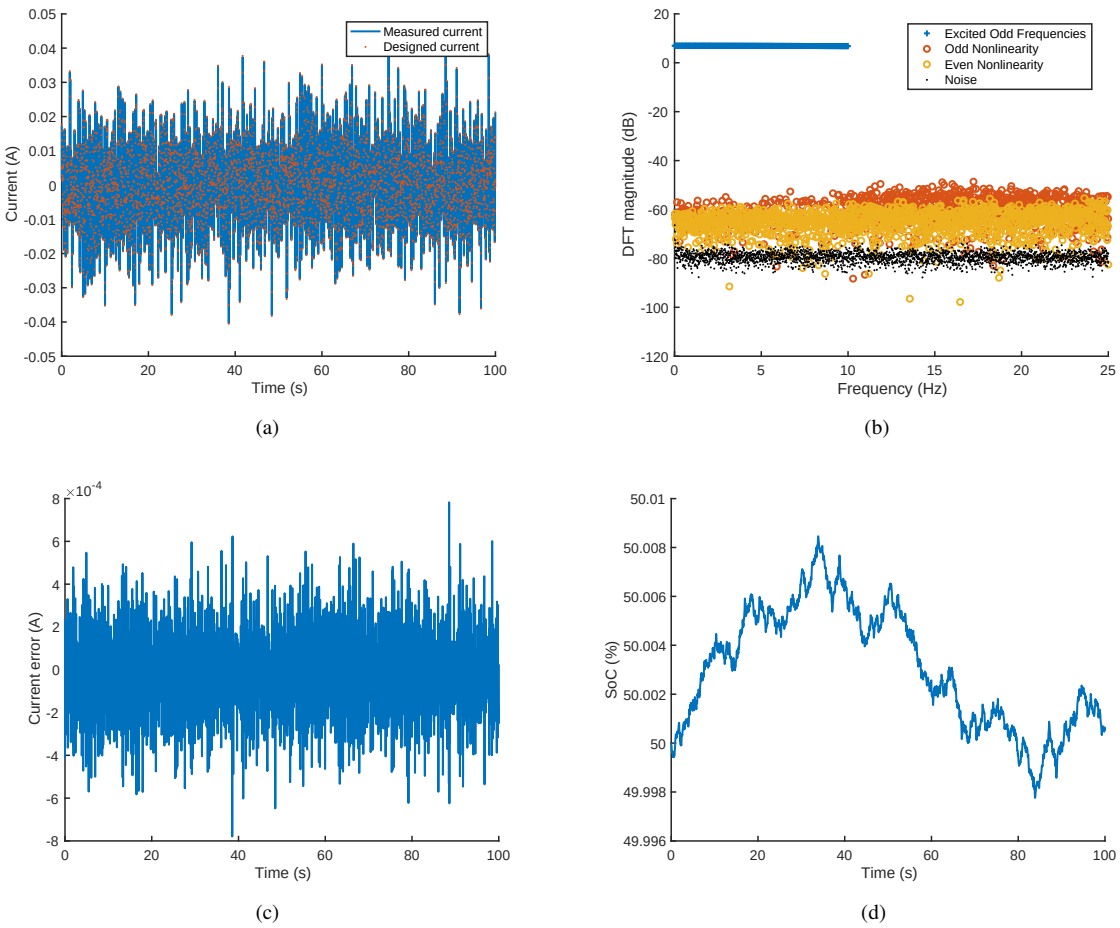

Fig. 1. (a) Measured and designed multisine current when the battery is at 50% SoC and 25 °C, (b) Frequency spectrum of measured multisine current, (c) Current error between measured and designed multisine, (d) SoC variation during multisine current.

2.2. Experiment setup

The battery load and open circuit voltage (OCV) data were recorded on a three-electrode configuration experimental PAT-Cell (EL-Cell) which was comprised of a 21.6 mm FS-5P separator (EL-Cell), 100 µl of R&D281 electrolyte (ethylene carbonate (EC) : ethylmethyl carbonate (EMC) 3:7 v/v + 1 wt% vinylene carbonate (VC) from Soulbrain), and the extracted positive electrode and negative electrodes punched into 18 mm disks. The electrodes (anode/cathode) were harvested from fresh 21700 LG M50 cylindrical cells following the teardown procedure [13]. Note the fresh cylindrical cells were purchased from the manufacturer and stored in a fridge (5 $^{\circ}C$) until they were discharged to 2.5 V and then disassembled. The reference electrode purchased from EL-Cell is comprised of a stainless steel ring that had lithium metal deposited on it. The extracted NMC 811 cathode and bi-component graphite-SiO_x anode had the coating on one-side removed to allow testing in a small format cell. The nominal rated capacity of EL-Cell in this study was 11.5 mA h, which also decides the magnitude of the 1 C-rate (1C) as 11.5 mA. Fig.2(a) shows the experimental setup for battery testing, which includes the three-electrode experimental EL-Cell, a charge and discharge test equipment (VMP3), a thermal chamber and a programmable upper computer. The battery was mounted in a thermal chamber at 25 °C for maintaining the cell surface temperature, and a VMP3 hardware was utilized to control the cell and record experimental data. The excitation current signals were programmed using the 'Batch Mode' function in the EC-Lab software (Bio-Logic®).

3. Nonlinear equivalent circuit model with diffusion dynamics (NLECM-diff) identification

3.1. Data-driven identification procedure

A lithium-ion battery is a nonlinear system exhibiting a non-linear voltage response caused by electrochemical behaviour when at different SoC levels and excitation input cases [36]. However, for conventional ECMs, any nonlinearity is commonly neglected and the interpretation of physical phenomena are discarded. This paper tries to develop a unique model, as shown in Fig.2(b), to associate the electrochemical behaviours in a lithium-ion battery, which consists of a linear equivalent circuit model for ohmic and polarization losses, a nonlinear sigmoid function for the nonlinear current-voltage relationship caused by the charge-transfer kinetics, an OCV-SOC block, and a simplified SoC dependent diffusion block for voltage loss caused by diffusion processes. The data-driven identification procedure and corresponding battery tests presented in Fig.2(c) is performed to fully characterize and validate the NLECM-diff model, including a OCV test for the OCV-SOC curve, multisine tests for the linear ECM and nonlinear sigmoid function), and a fully constant current (CC) discharge test for the SOC dependent diffusion block). Following that, three CC discharge and CC-CV charge tests, as well as a NEDC test, are performed to validate the proposed model. The following subsections describe the identification steps of the corresponding model blocks in detail.

3.2. Impedance estimate and equivalent circuit transfer function

For a lithium-ion battery, its impedance is commonly recognized as the linear part of battery dynamics response [24]. In the first step, an equivalent circuit model (ECM) is estimated by fitting the model parameters based on

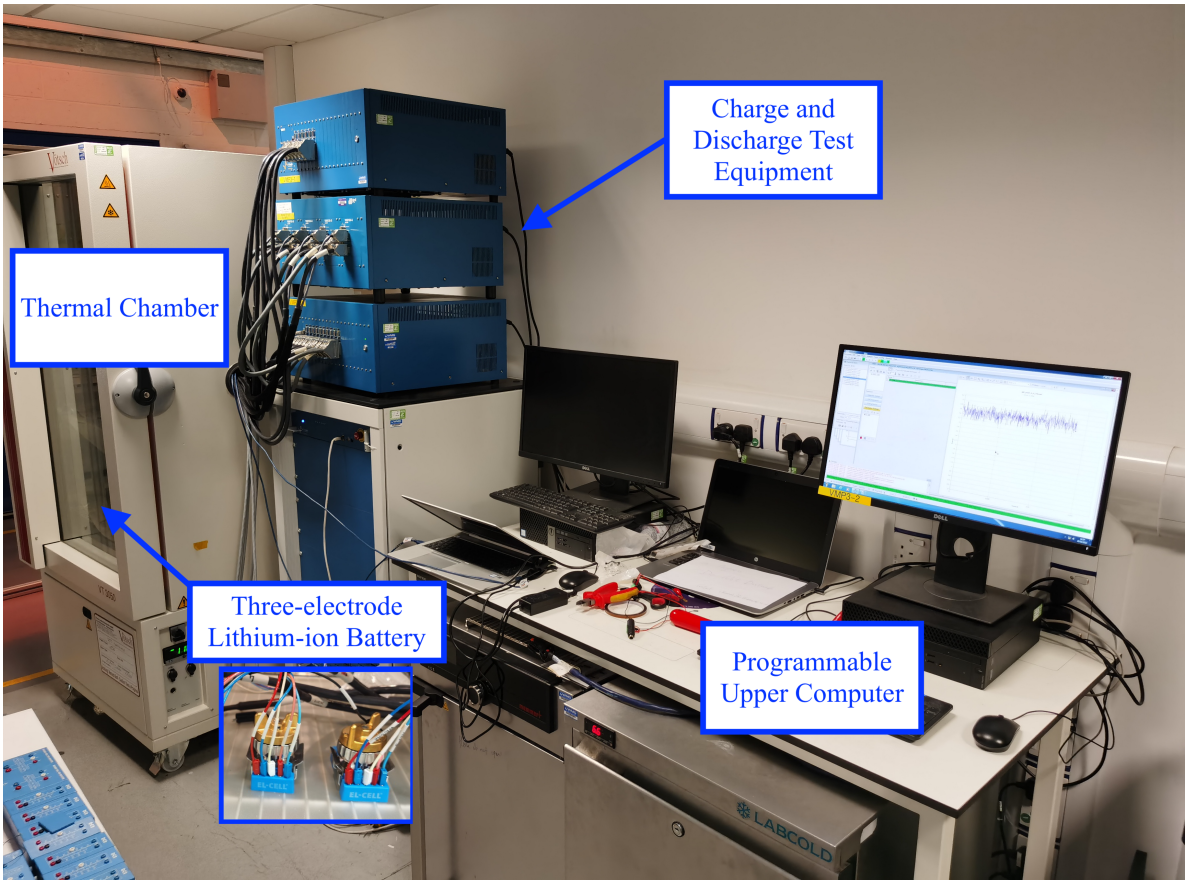

(a)

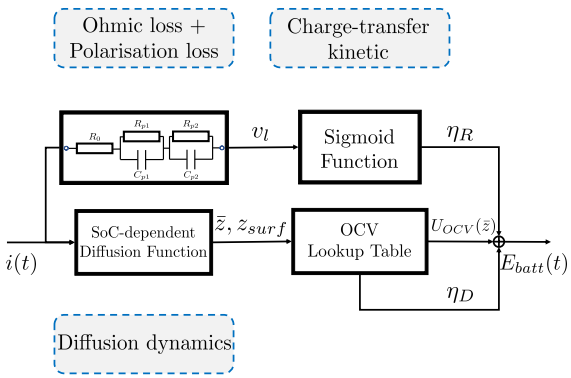

(b)

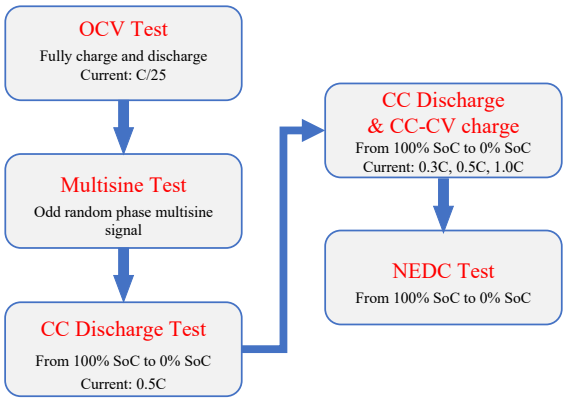

(c)

Fig. 2. Data driven identification approach and battery testing: (a) Experimental setup, (b) Lithium-ion battery NLECM-diff structure. The overall model consists of a linear ECM followed by a non-linear overpotential function, a parallel OCV block, and a parallel diffusion block, and (c) Flowchart of the data-driven identification procedure and the corresponding battery tests.

the best linear approximation from the measured current and voltage dataset. With the assistance of the periodic characteristic of multisine signal, a non-parametric function of battery impedance estimate can be obtained [43]. To acquire an accurate impedance estimate under steady-state conditions, the first three periods of the measured dataset are discarded to reduce the influence of any transient behaviour. Considering the discretized current and voltage measurement data in the remaining $P-3$ periods, we can obtain the averaged data over periods as:

$$\bar{i}(n) = \frac{1}{P-3}\sum_{p=4}^{P} i^{[p]}(n), \quad \bar{v}(n) = \frac{1}{P-3}\sum_{p=4}^{P} v^{[p]}(n) \qquad n = 0, 1, ..., N-1 \tag{3}$$

Where p indicates the pth period of the current $i(n)$ and the voltage data $v(n)$ measured at a given SoC.

As the thermodynamics will be accounted for by the OCV block and the diffusion process has no effect on voltage output during each multisine test when the SoC change is minimal, the *over-potential*, denoted as $\bar{v}_0(n)$, can be calculated by removing the mean voltage at the corresponding SoC from $\bar{v}(n)$ prior to estimating the impedance [24].

$$\bar{v}_0(n) = \bar{v}(n) - \frac{1}{N}\sum_{n=0}^{N-1} \bar{v}(n) \tag{4}$$

Then, by the Discrete Fourier transform (DFT), the time domain measured data can be transformed to frequency domain, termed as current and voltage spectra of pth period:

$$I(k), \quad V(k) \qquad k = 0, 1, ..., N-1 \tag{5}$$

where $I(k)$, $V(k)$ in Eq.(5) denote the DFT of $\bar{i}(n)$, $\bar{v}_0(n)$ at the kth harmonic.

In the frequency domain, the relationship between DFT voltage $V(k)$ and the DFT current $I(k)$ through the battery impedance $Z(k)$ is

$$V(k) = Z(k) \times I(k) + E(k) \tag{6}$$

Where $E(k)$ indicates the summation of error from any practical environment and distortion from non-linear battery behaviour.

The spectrum of over-potential $V(k)$ in the frequency domain at 10% SoC with 1C multisine current input is presented in Fig.3(a). Odd random phase multisine enables us to separate and quantify the odd and even nonlinearities through suppressed harmonics $H_{supp,odd}$ and $H_{supp,even}$, which can provide further insight about lithium-ion battery

non-linear behaviour. Details on the non-linear characterization method can be found in Ref. [36]. As shown in Fig.3(b), given $V(k)$ in Fig.3(a) and $I(k)$ in Fig.1(b), both the impedance $Z(k)$ and standard deviation $E(k)$ in the excited frequency range (10 mHz to 10 Hz) can be estimated by minimising the error term using the local-polynomial method (LPM) [24, 44]. The estimated impedance to standard deviation ratio is more than 25 dB, which indicates the high confidence of this impedance estimation.

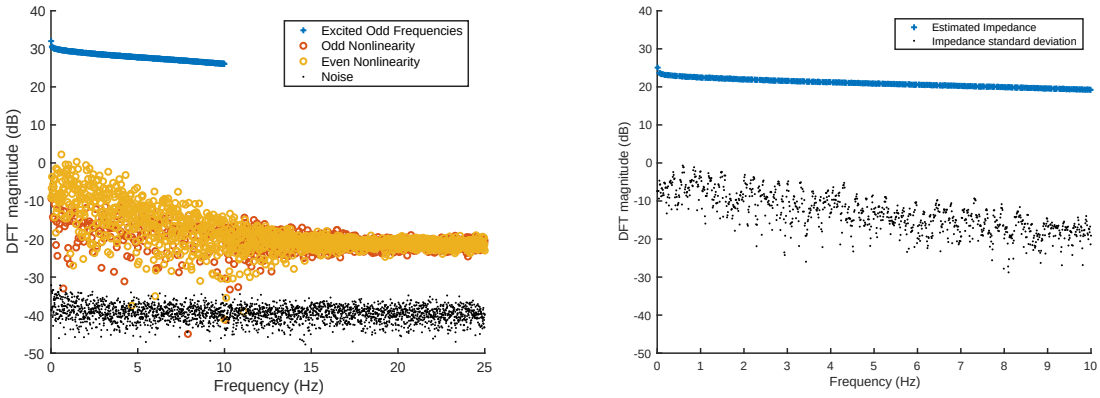

(a) (b)

Fig. 3. Spectrum of multisine characterised voltage and estimated impedance in the frequency domain: (a) Over-potential spectrum in the full frequency range, and (b) Estimated impedance and standard deviation in the excited frequency range at 10% SoC of an experimental cell.

Then, a transfer function is fitted to the estimated impedance.

$$Z_m(k) = \frac{b_{nb}(j\omega_k)^{nb} + ... + b_1 j\omega_k + b_0}{(j\omega_k)^{nb} + ... + a_1 j\omega_k + a_0} \tag{7}$$

Where $Z_m(k)$ denotes a transfer function mode, $\omega_k = 2\pi k f_s/N$ is the discrete angular frequency at harmonic k, and nb is the model order. The coefficients of Eq.(7) can be identified by minimising the error between the transfer function output and the estimated impedance. In this work, the Frequency domain System Identification Toolbox in Matlab® is applied to estimate transfer function coefficients [45].

Fig.4 shows the 1st and 2nd order transfer function fits of the impedance which indicates that the 2nd order model has a better agreement between the estimated impedance and fit than the 1st order. Note that both fits cannot perfectly match the impedance at few extreme low frequencies, which might be a limitation of the wide bandwidth multisine excitation. Unlike the previous literature Ref. [24, 30] only focusing on the extreme low frequency range ($\leq$ 1 Hz), the bandwidth in this work was extended to 10 Hz to comprise characteristic frequency ranges of both diffusion process and charge transfer kinetics. A rapid decrease in the impedance magnitude and a peak in the phase at low frequency range are shown in Fig.4, which is a phenomenon which has not been found in previous work. Given that

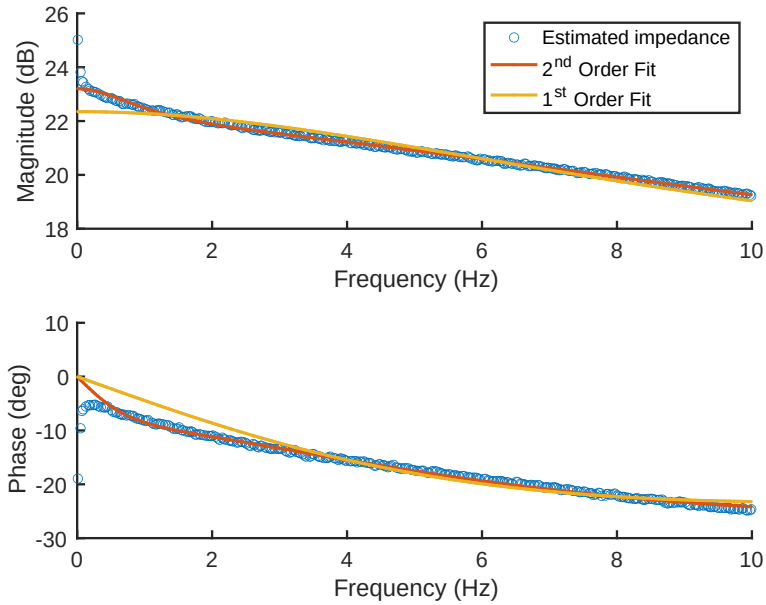

Fig. 4. 1st and 2nd order transfer functions for impedance estimated of the cell at 10% SoC.

its low characteristic frequency range, such a response might be attributed to diffusion process [46]. Although it leads the difficulty to fit all frequencies using 1st and 2nd order transfer function, a diffusion block will subsequently be introduced and coupled to compromise the influence caused by the phenomenon.

In addition, using orders greater than two generally generated better fits, however, the higher order model in this work result in positive poles which indicates an unstable system, and conjugate negative poles which is not possible to be implemented in practical applications. Therefore, the model order is selected as two in this work and the corresponding ECM is shown in Fig.2(b). Furthermore, in order to get the circuit parameters of an equivalent circuit model, the transfer function has to be expanded by a partial fraction expansion as shown in Eq.(8).

$$Z_m(k) = -R_0 - \frac{R_{p1}}{\tau_1 j\omega_k + 1} - \frac{R_{p2}}{\tau_2 j\omega_k + 1} \tag{8}$$

where R_0 denotes the internal ohmic resistance, R_{p1} and R_{p2} the polarisation resistances and τ_1 and τ_2 the time constants. The capacitances shown in Fig.2(b) can be obtained as $C_{p1} = \tau_1/R_{p1}$ and $C_{p2} = \tau_2/R_{p2}$.

Thus, the linear voltage losses $v_l(t)$ due to the ohmic and polarisation can be simulated with the corresponding 2nd order ECM with respect to a time-dependent current load $i(t)$ as Eq.(9).

$$v_l(t) = \mathrm{ECM}[i(t)] \tag{9}$$

3.3. Non-linear over-potential function

The non-linear over-potential function $f(v_l)$ shown in Fig.2(b) is inspired by the charge-transfer reaction in electromechanical kinetics. The Butler-Volmer equation, which relates the over-potential η_{ct} of an electrode to the current density $I_{batt}(t)$, is commonly utilized to represent the charge-transfer kinetics in electrochemical models [10, 15], as shown in Eq.(10).

$$\eta_{ct} = \frac{2RT}{F} \sinh^{-1}(\frac{I_{batt}(t)}{2i_0}) \tag{10}$$

where R is the molar gas constant, F is Faraday's constant, T the temperature and i_0 the exchange current. Eq.(10) represents the non-linear relation between current and over-potential, which is seldom interpreted in conventional battery ECMs. By plotting the measured over-potential $\bar{v}_0$ against the modelled ECM output $v_l(t)$ at each SoC, the presence of any non-linear deviations can be examined and captured through a non-linear function [24].

The over-potential data points and non-linear function fitting of the battery at 10% SoC are plotted in Fig.5. The blue "curve" formed by compact data points represents the non-linear characteristic of over-potential which shows a weak non-linear dependence in this study. Such a phenomenon is expected because, refer to Ref.[24], the strong non-linear dependency is only shown at low temperature (i.e. 0 °C) while a linear dependence is observed at 25 °C, which might be the reason that many conventional ECMs neglect the non-linearity during modelling. A non-linear function is used to estimate such phenomena, and the good agreement between the data points and the fit indicates non-linear deviations are well captured.

Given that the "S"-shape characteristic of the ideal Butler-Volmer kinetics (using symmetry anodic and cathodic charge-transfer factors equal to 0.5), a sigmoid function is used to model the non-linear characteristic as its bounded and differentiable features can ensure the function convergence. Note that, refer to recent research Ref.[47], the anodic and cathodic charge-transfer factors may be not symmetrical in a practical lithium-ion battery, which leads to more possibilities including the polynomials and logistic functions that should be considered to model the non-linear phenomena. Impact of model function selection is still an open question and will be studied in the future work.

In this study, the non-linear voltage loss $\eta_R(\bar{v}_l)$, caused by ohmic, polarisation and possible non-linear effects is obtained by the following sigmoid function, which is used to fit the measured ($\bar{v}_0$) against modelled average linear over-potential $\bar{v}_I$ data

$$\eta_R(\bar{v}_l) = \frac{c_1 \bar{v}_l}{\sqrt{1 + c_2 \bar{v}_l^2}} \tag{11}$$

where c_1 is the linear and c_2 is the non-linear sigmoid coefficients in Eq.(11). The *lsqcurvefit* function from the Matlab® Optimisation Toolbox is used to estimate two sigmoid coefficient at each SoC. Then, a linear look-up table

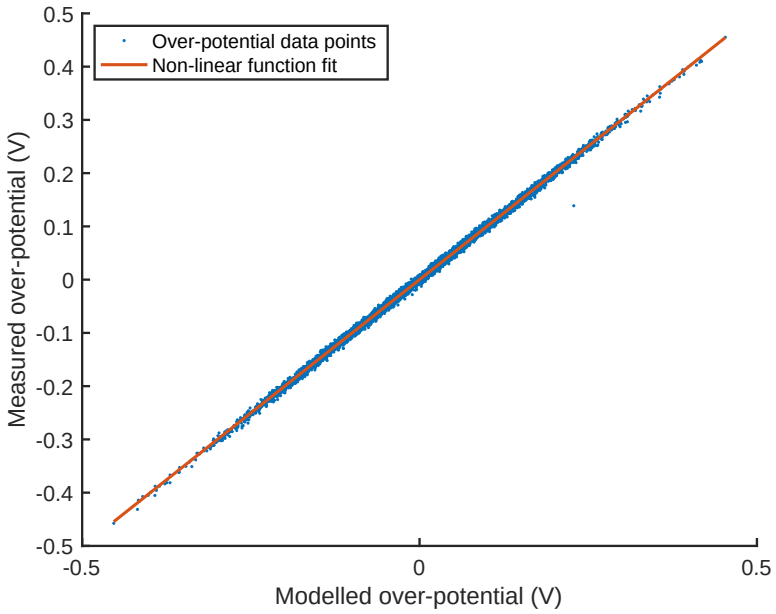

Fig. 5. The non-linear characteristic and non-linear function fitting at 10% SoC and 25 °C.

of the estimated coefficients at each SoC is built up for model simulation.

3.4. Open circuit voltage (OCV) block

From electrochemical point of view, the battery open circuit voltage U_{OCV} accounting for thermodynamic is related to the potential of the cathode $U_c(\bar{c}_c)$ and anode $U_a(\bar{c}_a)$, as shown in Eq.(12), which depends separately on the bulk average lithium concentration of individual electrode particles ($\bar{c}_c$ and $\bar{c}_a$).

$$U_{OCV} = U_c(\bar{c}_c) - U_a(\bar{c}_a) \tag{12}$$

For modelling purposes, the SPMe model assumes the size and dynamics of electrode particles to be identical within an electrode; Consequently, the cathode and anode can be treated as two electrode particles [15]. Thus, the battery macroscopic SoC is defined as the ratio of the average usable lithium ion concentration $\bar{c}$ to the maximum usable lithium ion concentration in the electrode particle in Eq.(13)

$$\bar{z} = \frac{\bar{c}_c - \bar{c}_{c,0\%}}{\bar{c}_{c,100\%} - \bar{c}_{c,0\%}} = \frac{\bar{c}_a - \bar{c}_{a,0\%}}{\bar{c}_{a,100\%} - \bar{c}_{a,0\%}} \tag{13}$$

where $\bar{c}_{100\%}$ indicates the battery is full (100% SoC) and $\bar{c}_{0\%}$ indicates the battery is empty (0% SoC). Then, the open circuit voltage U_{OCV} can be related to the average SoC $\bar{z}$ which is represented as a $\bar{z}$-U_{OCV} curve in battery

models.

In the battery modelling procedure, an extreme low current (usually C/25), which theoretically can minimise any battery polarization, is applied to fully charge and discharge the battery, and the $\bar{z}$-U_{OCV} curve, termed as pseudo-OCV, can be estimated by averaging the measured charge and discharge voltage curves [48]. In this work, the three-electrode cell is employed to record not only the OCV of the full-cell (U_{OCV}) but also that of the cathode and anode (U_c, U_a). Then a *Look-Up Table* is used to archived each OCV curve to act as the open circuit voltage block in the model.

Up to this point in the paper an NLECM similar to that proposed in Ref.[24] consisting of a linear ECM block, a non-linear over-potential block, and an OCV block with respect to the macroscopic SoC achieved by current integration method, has been identified and parametrized by applying a multisine excitation at each SoC, and the performance of the NLECM will be reported and used for comparison in Section 3.6.

3.5. SoC dependent diffusion block

When a battery is in operation, due to the diffusion processes, the distribution of lithium ion concentration in the particle is not uniform [49]. Thus, the open circuit voltage $U(t)$ is directly reflected by the lithium ion concentration at the particle surface ($c_{c,surf}$ and $c_{a,surf}$), i.e. cathode surface potential $U_c(c_{c,surf})$ and anode surface potential $U_a(c_{a,surf})$, in which the potential subtraction is noted as $\triangle U_{surf}$. Refer to Ref.[33], in order to design the proposed model more suitable for BMS applications, the relationship between the potential subtraction $\triangle U_{surf}$ and the particle surface lithium concentration c_{surf} during operation can be approximated by the $\bar{z}$-U_{OCV} curve with the surface SoC, noted as z_{surf}, as the input. Thus $\triangle U_{surf}$ can be represented as shown in Eq.(14)

$$\triangle U_{surf} = U_c(c_{c,surf}) - U_a(c_{a,surf}) = U_{OCV}(z_{surf}) \tag{14}$$

Furthermore, the diffusion voltage loss η_D related to the difference of average concentration and surface concentration in solid-phase diffusion process could be written as Eq.(15).

$$\eta_D = U_{OCV}(\bar{z}) - U_{OCV}(z_{surf}) \tag{15}$$

However, the conventional ECM commonly neglects the diffusion processes inside particles and only represents the open circuit voltage by using a simple DC power source which results in poor model accuracy over the whole SoC range, especially at low SoC range [50]. Therefore, a simplified SoC dependent diffusion block is introduced in this section to account for the diffusion voltage loss η_D. It is noted that the aforementioned ECM and nonlinear function are identified by multisine characterisation testing that is designed to minimize battery SoC change to a minimum during operations, thus no voltage loss caused by the diffusion process is taken into account. Such that the large time

constant dynamics associated with the diffusion process and the small time constant dynamics associated with ohmic and charge-transfer kinetics are decoupled for easy identification.

To interpret the variation in average and surface SoC caused by diffusion process using a simplified mathematical representation, the diffusion equation solving SoC variable z for a battery particle, refer to Ref.[34], is defined on a one-dimensional geometry, using a dimensionless variable x ranging from 0 (centre of the particle) to 1 (surface of the particle) according to the following partial differential equation

$$\tau_d \frac{\partial z}{\partial t} - \frac{\partial^2 z}{\partial x^2} = 0 \tag{16}$$

where τ is a time constant which is related to the diffusion coefficient determined by battery chemical materials and manufacturing process.

The boundary conditions are

$$\left.\frac{\partial z}{\partial x}\right|_{x=0} = 0, \qquad \left.\frac{\partial z}{\partial x}\right|_{x=1} = \frac{\tau_d i(t)}{Q} \tag{17}$$

where Q is the parameter corresponding to the battery capacity. The diffusion block is only implemented in the Cartesian coordinate system in this work, and the other coordinate dimensions are not studied here, but, refer to Ref.[34], only a minor impact is shown when using different coordinate systems.

To solve Eq.(16) with low computational cost, a Chebyshev pseudo-spectral method, termed as the discrete Chebyshev-Gauss-Lobatto (CGL) orthogonal collocation method, is applied in this work [51]. Unlike the finite difference method in Ref.[52] and the finite element method in Ref.[53] which require very high spatial resolution, the pseudo-spectral method is a global method which uses all available function values to construct the necessary approximations to simplify calculation while retaining interpretability [54], making it well-suited for our case and BMS applications. With the orthogonal collocation method, it is possible to find the SoC variable $z(t, 0 \leq x \leq 1)$ at the grid points $x_j = (1 + \cos(j\pi/N))/2$, $j = 0, ..., N$, which distributes in the battery particle from the centre to the surface, by solving the following system of $(N + 1)$ differential algebraic equations (DAEs):

$$\begin{cases} \dfrac{\partial z_j(t)}{\partial t} = 4 \sum\limits_{k=0}^{N} b_{jk} z_k(t), \qquad j = 1, ..., N-1 \\ z_0(t) = 0 \\ z_N(t) = \dfrac{\tau_d i(t)}{Q} \end{cases} \tag{18}$$

where $D^2 = D \cdot D = (b_{jk})_{0 \leq j \leq N, 0 \leq k \leq N}$ is the square of the derivative matrix D, and N is arbitrarily selected as 6 in

this study. Details on the CGL orthogonal collocation method are found in Ref.[55], while a brief description of the procedure is presented in Appendix A.

In the diffusion block, the surface SoC z_{surf} can be directly obtained from Eq.(16) while the grid point at surface is selected, as well as the average SoC $\bar{z}$ of the battery particle in this work can be obtained by

$$\bar{z} = \int_0^1 z \partial x \tag{19}$$

The voltage loss of SoC dependent diffusion block η_D in Eq.(15) is now available for the NLECM-diff model.

To estimate Q and τ_d of the diffusion block, a global optimization method, named simulated annealing algorithm (SA) proposed by Kirkpatrick [56], is applied here for the model parametrization. The approach of the SA to estimate the optimum parameters is minimizing the cost function (J) defined as the sum of the weighted squared error between voltage measurement and the NLECM-diff model output voltage.

$$J = \sum \left| \frac{v(t) - v_m(t)}{\sigma_{v(t)}} \right|^2 \tag{20}$$

In Eq.(20), $v(t)$ is the voltage measurement, $v_m(t)$ is the model-calculated voltage, and the $\sigma_{v(t)}$ is the standard deviation of the voltage measurement. Given that the diffusion process is a long time operation [32], a parametrization process under a long time profile (separate and in addition to the multisine characterisation experiments) is required for the NLECM-diff. Thus, the optimisation is based on a 5.75 mA (0.5C) constant current (CC) discharge experiment (from 4.2 V to 2.5 V) followed by a 4 h relaxation at 25 °C, and the optimized model fit will be reported in Section 3.6. During the optimization process, the results show that the voltage response during the discharge period, especially the ending estimated voltage value, depends on the diffusion-related time constant τ_d, which is determined as 1350 for the full cell model. Note that, refer to [13], the diffusion coefficient is a SOC-dependent parameter, however, to keep the simplicity of the parameterisation process, τ_d is assumed to be a constant over the whole SOC range in this work. Furthermore, the final estimated voltage value in the relaxation is strongly related to Q, and the Q is determined to equal to 0.0113 which is close to the rated capacity of the battery 0.0115 A h .

By coupling the identified NLECM and the SoC-dependent diffusion block, the NLECM-diff, which accounts for key battery dynamics, including the ohmic response, the charge-transfer kinetics, and the diffusion process, is accomplished. The model defines the time-dependent voltage E_{batt} when subject to a time-dependent battery current load using the Eq.(21), and all nine parameters of the proposed model are listed in Table 1.

$$E_{batt} = U_{OCV}(\bar{z}) + \eta_R + \eta_D \tag{21}$$

Table 1
Summary of NLECM-diff model parameters and related characterization methods.

Parameters	Description	Characterization methods	Unit
R_0	Ohmic resistance	Multisine test	Ω
R_{p1}	Resistance of the first polarization process	Multisine test	Ω
τ_1	Time constant of the first polarization process	Multisine test	s
R_{p2}	Resistance of the second polarization process	Multisine test	Ω
τ_2	Time constant of the second polarization process	Multisine test	s
c_1	Linear coefficient of sigmoid function	Multisine test	–
c_2	Non-linear coefficient of sigmoid function	Multisine test	–
U	Open circuit voltage	pseudo-OCV test	V
Q	Parameter corresponding to the battery capacity	C/2 discharge test	A h
τ_d	Time constant of diffusion process	C/2 discharge test	s

3.6. Comparison between NLECM-diff and NLECM

To quantify the advantage over an NLECM, the accuracy of the proposed NLECM-diff and the NLECM is compared under different load profiles in this section. Note that, as the accuracy of the NLECM is demonstrated to be superior to that of traditional ECMs [24], only the NLECM is taken into consideration in this work.

Fig.6(a) and Fig.6(c) show the voltage estimation and voltage error results under a multisine excitation current when the battery is at 50% SoC. Note that the measured multisine dataset here is not the one used for the model identification. The results show that the voltage estimation of the two models almost overlap the experimental data and that most of voltage error is smaller than 0.02 V. Furthermore, the goodness-of-fit R^2 and voltage root mean square error, which are widely used metrics for model performance evaluation, of the NLECM and NLECM-diff under the two testing profiles are listed in Table 2. The R^2 value of the NLECM-diff result is 99.67% which is 0.01% higher than the NLECM, while the RMSE value of NLECM-diff is 0.0006 V less than that of the NLECM. The high R^2 and small RMSE value indicate both the NLECM and the NLECM-diff have great precision under the multisine test, while the minor difference between these two metrics imply that the accuracy of two models are really close.

Furthermore, the accuracy of two models is evaluated using a 0.5C constant current discharge with relaxation profile, as illustrated in Fig.6(b). Compared with the significant deviation of the NLECM results, a good agreement between the NLECM-diff results and the experimental data is clearly observed. Moreover, when the discharge profile ends, the NLECM-diff can smoothly transit into the relaxation status (as black array shown), however, the NLECM voltage response directly changes to a flat straight line after an instant ohmic voltage recovery. Additionally, as shown in Fig.6(d), although the voltage error slightly increases at the low SoC range during the discharge profile, the maximum voltage error is less than 0.15 V and the final voltage value converges to the experimental result in the relaxation process, which indicates the high accuracy of the NLECM-diff through the whole SoC range. In contrary,

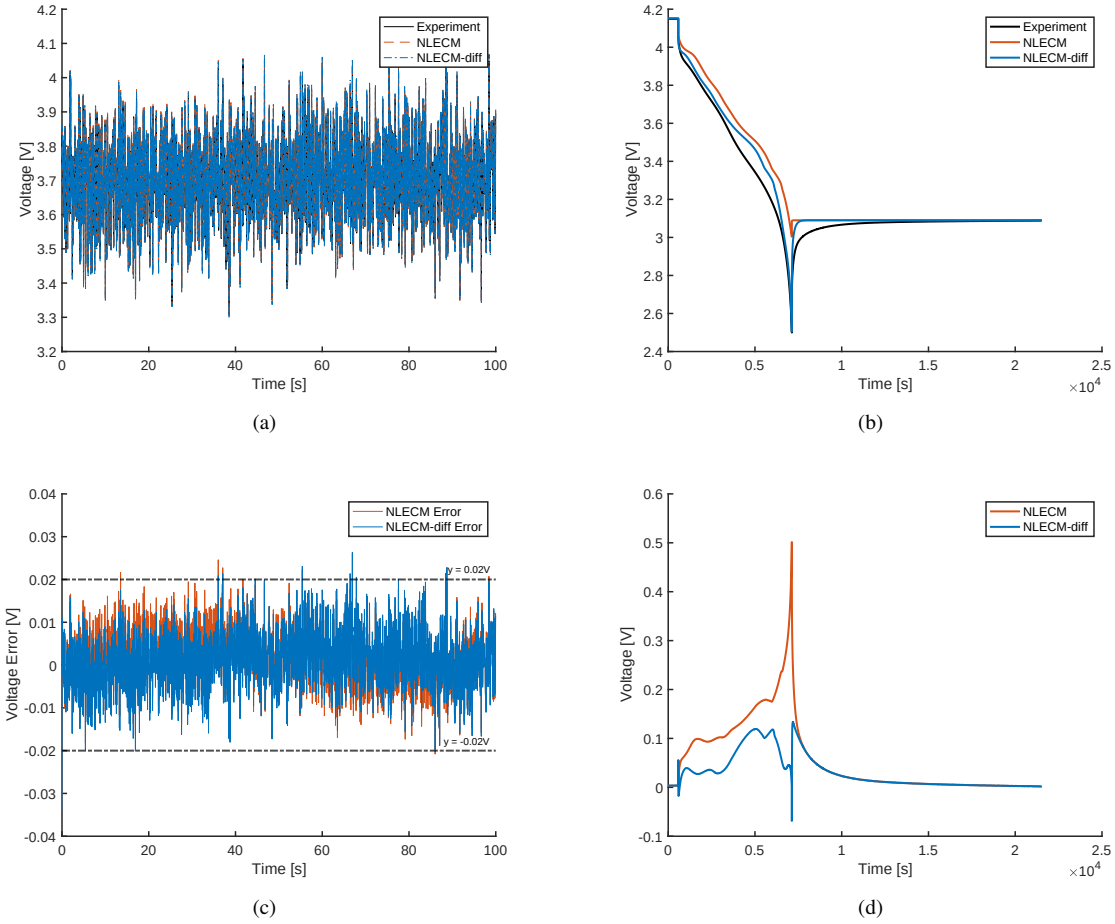

Fig. 6. Comparison between NLECM and NLECM-diff under when subjected to a different load profiles. (a,c) Voltage estimation and voltage error results under multisine current at 50% SoC, and (b,d) Voltage estimation and voltage error results under a 0.5C constant current discharge followed by a 4 h relaxation.

the NLECM results deviated from the experimental data from the beginning of discharge and the error increases to around 0.75 V, which illustrates the drawback of the NLECM, especially in the low SoC range. Such phenomena demonstrate the NLECM-diff's advantage of capturing diffusion dynamics and the importance of a diffusion process block in a battery model for long time discharge operation. In addition, according to Table 2, the NLECM-diff could reduce the voltage RMSE by more than 49.6% and improve the R^2 values by 4.6% when compared to NLECM, which indicates the significant accuracy improvement of NLECM-diff compared to the traditional NLECM in the 0.5C CC discharge test.

From a parametrization point of view, only two extra parameters (Q and τ_d) are added in the NLECM-diff, resulting in relatively limited increase of the cost in parameter identification. No experimental methods and chemical analysis are involved in the identification of the NLECM-diff which provides a promising modelling pattern for the battery management system (BMS) developers without specific electrochemical techniques. Furthermore, the introduction

Table 2
Goodness-of-fit (R^2), voltage RMSE, and maximum error comparison of NLECM and NLECM-diff in the multisine and 0.5C CC discharge tests.

	Multisine Test			CC Discharge		
	R^2 [%]	RMSE [V]	Maximum Error [V]	R^2 [%]	RMSE [V]	Maximum Error [V]
NLECM	99.66	0.002	0.026	94.05	0.093	0.504
NLECM-diff	99.67	0.001	0.025	98.65	0.047	0.076

of the diffusion process block accounts for the potential variation inside the battery electrode particles, such that an evident accuracy improvement under long time operation profiles could be made by the NLECM-diff, in contrast to the NLECM and even the traditional ECM only contains the OCV block with respect to the average SoC.

4. Model validation and results discussion

In this section, the voltage estimation accuracy of the NLECM-diff model, which is identified using the methodology presented in Section 3, is validated under various load profiles. Taking advantage of the reference electrode instrumentation, the NLECM-diff model is developed not only for the full cell to emulate the battery terminal voltage dynamics, but also for the individual electrodes, labelled as NLECM-diff (PE) for the positive electrode and NLECM-diff (NE) for the negative electrode. Section 4.1 presents that the applicability of the NLECM-diff model on the prediction of the electrode potential response, which is compared to the single particle model with electrolyte dynamics (SPMe) proposed in Ref.[15] with a constant current (CC) discharge and constant current-constant voltage (CC-CV) charge tests. Furthermore, to validate the model effectiveness for a full cell in a variety of operational scenarios, the aforementioned CC discharge CC-CV charge tests and the New European Driving Cycle (NEDC) experimental test are conducted in the validation procedure to examine and compare the accuracy of the NLECM-diff model and the SPMe in Section 4.2 and 4.3, respectively. Note that, in this study, the partial differential equations in the SPMe are solved by the finite difference method, as well as the parameters in the SPMe are from a published paper which utilizes experimental methodologies to obtain the related parameters of the same NMC chemistry cell and their accuracy and validity have been discussed in Ref.[13]. Lastly, the dominant battery phenomenological behaviours in terms of voltage losses under different load profiles are found by the NLECM-diff and reported in Section 4.4.

4.1. Results under CC discharge and CC-CV charge profiles - Individual Electrodes

An essential feature of electrochemical models is that the dynamic response of individual electrodes can be predicted, which can be employed to estimate internal potential variables for practical applications, such as charging strategy optimization. For instance, the cells' current can be controlled during charging in a way to maintain the potential of negative electrode above 0 V vs. Li/Li^+ to prevent lithium plating [57]. However, the extensive parameterisation procedure, related to the geometrical and kinetic dynamics, of electrochemical models introduce difficulty

for practical applications. Using three-electrode configuration experimental cells with a lithium reference electrode, the positive and negative electrode potential can be measured simultaneously. On the basis of the measured electrode potential and excitation current signal, the NLECM-diff model can be more easily developed (as discussed in Section 3) for individual electrodes to achieve same objectives by using electrochemical models. This section evaluates the potential response accuracy of de-coupled electrode NLECM-diff models in comparison with the experimental measured data and the potential estimation from the SPMe.

The performance of the NLECM-diff is evaluated under a set of constant current (CC) discharge and constant current-constant voltage (CC-CV) charge profiles. The profile is determined as a two-period cycle, in which the battery experiences constant current discharge until the lowest cut-off voltage followed by a relaxation for 4 h in the first period, and, in the second period, a 0.3C constant current charge is applied at the beginning and when the voltage reaches a threshold value, the battery will be charged by the CV charging method until the charge voltage limit. The long constant-current discharge period is used to simulate stable driving conditions with relatively constant speed and demand, the rest period is used to verify the accuracy of the voltage estimation during the depolarization process, and the CC-CV charge period is used to evaluate the model's performance under a widely used battery charging strategy. Three different current discharge tests were conducted, that include 3.83 mA (0.3C), 5.75 mA (0.5C), and 11.5 mA (1C), to discharge the battery from 4.2 V (Max rated voltage) to 2.5 V (Min rated voltage) in order to examine the impact of discharge rates on model accuracy throughout the whole voltage window, and the other parts of the profiles remain consistent.

Fig.7 shows the results of the model voltage and voltage error of the SPMe and the NLECM-diff models for the positive electrode (PE) and negative electrode (NE) in comparison with experimental measurements in CC discharge and CC-CV charge tests with different discharging current rates. It is worth noting that the model simulations use the same excitation current signal as recorded in the experiments. The measured experimental data (black line) of the positive electrode potential for 0.3C, 0.5C, and 1C discharging scenarios are plotted in Fig.7(a), 7(b) and 7(c). Both SPMe (PE) in blue line and NLECM-diff (PE) in red line can obtain a high degree of agreement with the experimental PE potential over the entire validation profiles. In the relaxation periods with no current excited, the gradually increasing potential of the positive electrode is observed in both models, and the model estimations at steady state are overlapped on the measured results. Furthermore, Fig.7(d), 7(e) and 7(f) present the model estimations and measured data of the NE potentials under the various discharging profiles. It can be observed that the NLECM-diff (NE) model in green dash line is consistent with the SPMe (NE) in yellow dash line among the three scenarios, there is however an overestimation from the SPMe (NE) at the end of discharge in 7(e). The voltage error of the NLECM-diff model is in good agreement with the SPMe results for each electrode and is mostly within the boundary range, which indicates that the accuracy of the NLECM-diff model is as high as the SPMe for electrode potential estimation. However, contrary to the accurate potential estimations obtained for positive electrode, the model estimated results of the negative electrode potential show the relatively large error in comparison with the experimental data.

The estimated voltage error of the positive and negative electrode models are plotted in Fig.7(g), 7(h), and 7(i).

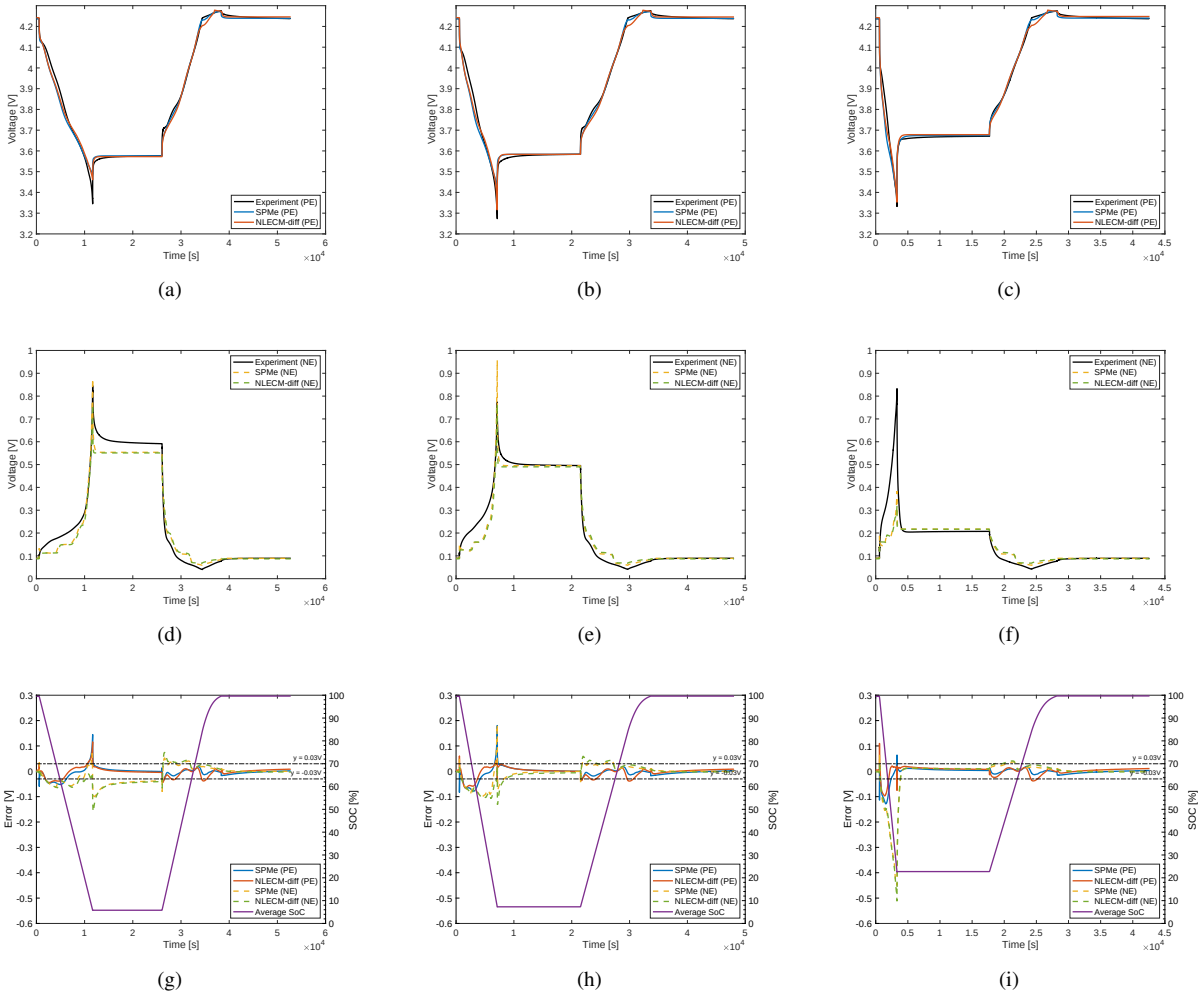

Fig. 7. Positive electrode (PE) and negative electrode (NE) potential estimations and voltage error results of SPMe and NLECM-diff (Electrode) in CC-CV discharge and charge test with different discharge current values: (a, d, g) under 0.3C discharge current; (b, e, h) under 0.5C discharge current; (c, f, i) under 1C discharge current.

Note that the error is determined by the measured value subtracted by the model estimated value under the same current input, such that a positive error indicates that model overestimate the voltage while a negative error implies underestimation. The black dashed lines in the voltage error figures reflect the 0.03 V and −0.03 V error boundaries. The results show that, when the cell discharges, the estimation error increases as the discharging current rate raises. The model results only show comparable small voltage error in the 0.3C and 0.5C cases, however, in the 1C case, a significant error comparing to experimental data can be noticed in the result of each model. It's worthy to note that the accuracy of the parameterised SPMe model has been validated in previous work [18]. Such that the NLECM-diff model can achieve a high degree of accuracy as SPMe model. During the CC-CV charge duration, all models can maintain a good accuracy within the boundary. In addition, Fig.7(g) presents the underestimation of estimated

positive and negative electrode potential during the discharge period, except the positive electrode potential at end of the period. It is worth to note that, during discharging, the larger voltage error of PE models is found in the middle of SoC range, as well as the significant voltage error of NE models is shown in the low SoC region. Furthermore, the error value of NE models is greater than that of the PE models in the low SoC area. The similar phenomena can be more obviously observed in Fig.7(h) and 7(i). The largest voltage error of positive electrode reaches around −0.09 V in the 0.5C case and −0.11 V in the 1C case at 65% SoC, and then, the voltage error gradually decreases until the end of discharging. For the negative electrode, it is shown that when the SoC decreases, the voltage inaccuracy increases. The voltage error can reach to −0.5 V at end of discharging in Fig.7(i), where the voltage error of positive electrode is almost negligible. Moreover, the NE potential in the SPMe with validated parameters also exhibits as large voltage error as the NLECM-diff (NE) model. Such results illustrate that the dominant voltage error source, which leads to poor accuracy of battery models in the low SoC region, is from the negative electrode rather than from the positive electrode.

In addition, the goodness-of-fit (R^2), voltage RMSE, and maximum error of electrode models under the long time discharge and charge profiles are compared and then listed in Table 3. It can be seen that, for two PE models, the maximum difference of R^2 is less than 0.15% and the maximum difference of RMSE values is less than 0.0054 V in all three validation scenarios, which indicates that the PE models can maintain high accuracy under various current density loads. Furthermore, the NLECM-diff (PE) model shows higher R^2 and lower RMSE than SPMe (PE), which suggests the proposed model is marginally more accurate than SPMe in the positive electrode case. On the other hand, the results describe that, in the negative electrode case, the NLECM-diff (NE) model accuracy is difficult to maintain under high current condition, as the R^2 value significantly drops from 96.82% in 0.5C test to 56.78% in the 1C test, as well as approximately 0.0349 V RMSE value 0.381 V maximum error increment exists while the 1C validation profile is applied in comparison with the 0.5C test. Moreover, the minor accuracy difference between the NLECM-diff (NE) model and the SPMe (NE) suggests that the fidelity of these two models is still comparable and the estimation error may be not due to the model inaccuracy.

Table 3
Accuracy of SPMe (PE), NLECM-diff (PE), SPMe (NE), and NLECM-diff (NE) in comparison with experimental results in long time CC discharge and CC-CV charge tests.

	Goodness-of-fit (R^2) [%]			RMSE [V]			Maximum Error [V]		
	0.3C	0.5C	1C	0.3C	0.5C	1C	0.3C	0.5C	1C
SPMe (PE)	99.43	99.31	99.46	0.022	0.026	0.020	0.145	0.180	0.128
NLECM-diff (PE)	99.66	99.65	99.58	0.017	0.018	0.018	0.116	0.064	0.096
SPMe (NE)	97.68	96.15	59.23	0.038	0.039	0.068	0.099	0.184	0.450
NLECM-diff (NE)	97.52	96.82	56.78	0.040	0.035	0.070	0.157	0.131	0.512

In this section, the modelling methodology presented in Section 3 is employed to develop the NLECM-diff model for both electrodes, and the performance of the electrode NLECM-diff models is compared with the SPMe. The results

indicate that these two models have comparable fidelity, to the point where the NLECM-diff model may be used in place of the SPMe for estimating the battery internal potential variable. Additionally, in comparison to the minor error associated with positive electrode models, both negative electrode models exhibit relatively large low-SoC-area error when is subjected to a high current load, which demonstrates that the negative electrode dynamic response may be the primary reason resulting in the inaccuracy of battery models in the low SoC region.

4.2. Results under CC discharge and CC-CV charge profiles - Full cell

To fulfil the requirement of general practical applications where access to the individual electrode potentials is not possible, a NLECM-diff model for a full cell is developed based on terminal voltage of the three-electrode experimental cell for simulating the dynamic response of commercial cells. The performance of the full cell NLECM-diff model is evaluated using the CC discharge and CC-CV charge profiles described in Section 4.1, and the NLECM-diff model's voltage response is compared to the SPMe's terminal voltage in this section.

Fig.8 presents the voltage estimation and error of the SPMe and the NLECM-diff model for a full cell in the various validation loads. The results under 0.3C discharge current are shown in Fig.8(a) which suggests both models provide minor voltage error at the high and middle SoC range with the errors less than 0.03 V. For SoC lower than 30%, the voltage error surpasses the the boundary, which indicates the model voltages are overestimated. During the discharge period, the voltage error of the NLECM-diff model is comparable to the SPMe results. Furthermore, when the battery transits to the relaxation period, the largest deviation from the measured voltage gradually decreases due to the battery diffusion process. It is also noticed that, the voltage error of the NLECM-diff model follows closely the SPMe results which indicates that the NLECM-diff model maintains a comparable fidelity as the SPMe. Moreover, in the 0.3C CC-CV charging period, both models underestimate the terminal voltage. Compared with the around 0.03 V error of SPMe during charging, the NLECM-diff model exhibits poorer accuracy with maximum 0.11 V estimated error. It might be caused due to the fact that the lumped SoC diffusion block, which is calibrated at 0.5C constant current discharge profile, is not suitable for the charge process. At the end of the validation test, the estimated voltage can converge to the measured value with less than 0.007 V error. Furthermore, the estimated voltage and error under the 0.5C CC discharge and CC-CV charge load are demonstrated in Fig.8(b). Similar to the electrode model results in the previous section, the error of the two models increases in the discharge period, especially in the low SoC range. The NLECM-diff model overestimates the terminal voltage, and its error is greater than that of SPMe (Max. 0.118 V versus Max. 0.087 V). However, the voltage error during relaxation are minor, even less than that in the 0.3C case, which might because the models were calibrated under the 0.5C discharge case. Same as the 0.3C case, the NLECM-diff voltage error in the relaxation period has a good agreement with that of the SPMe at around 0.002 V. Lastly, Fig.8(c) shows the estimated results of two models in the 1C discharge case where the voltage error remains within the boundaries at the start of discharge, but the large deviation from the experiential data appears from 64% SoC in the discharge process. Not only the NLECM-diff model, the SPMe exhibits a significant voltage error in the low SoC range. Furthermore, it is to noticed that, according to the average SoC (purple line) obtained by current integration

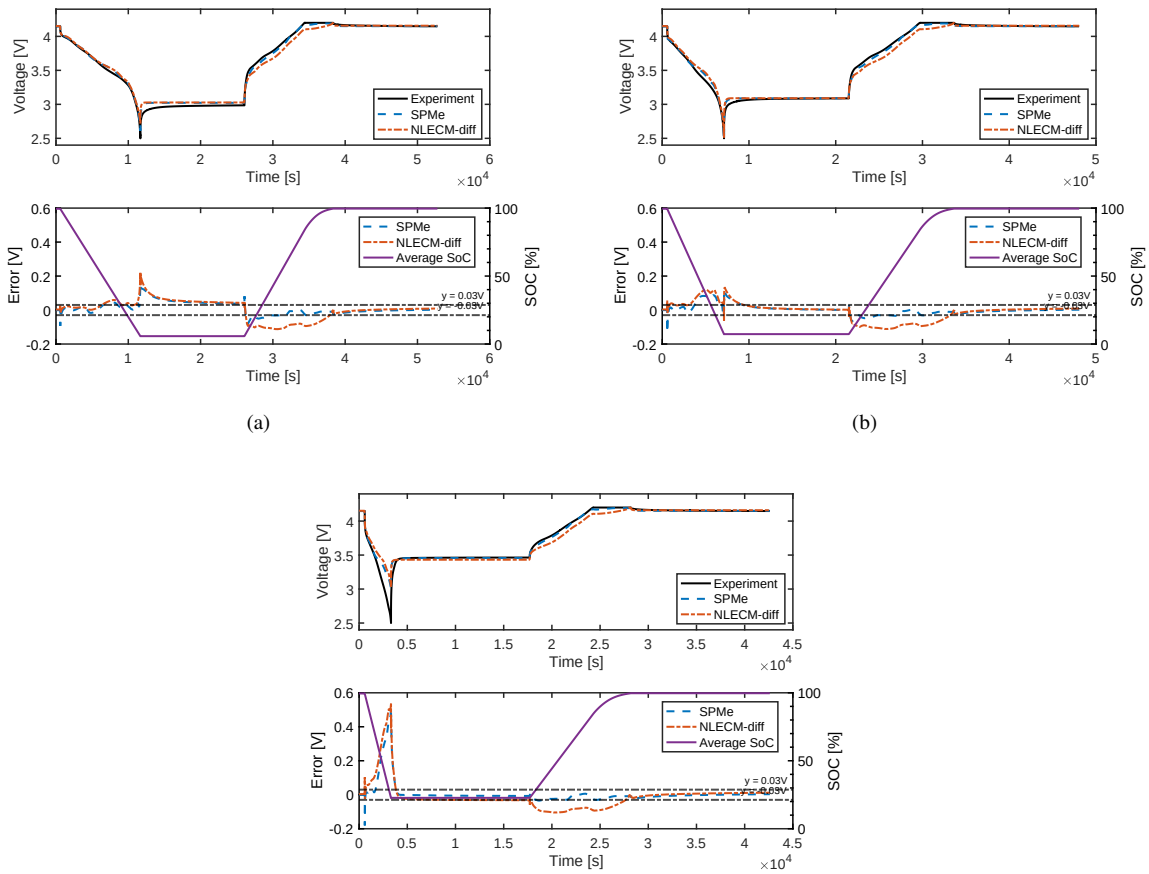

Fig. 8. Voltage estimation and voltage error results of the SPMe and the NLECM-diff model for a full cell in CC-CV discharge and charge test with different discharge current values: (a) under 0.3C discharge current; (b) under 0.5C discharge current; (c) under 1C discharge current.

method, when the experimental battery voltage is discharged to the minimum limit 2.5 V under 1C constant current, the average SoC only reaches to 22.8% rather than to around 0% in expectation. The dominant battery process which results in a significant error in the low SoC range as well as the unexpected SoC variation will be discussed in Section 4.4. Interestingly, the error magnitude of the full cell models is consistent with that of the negative electrode models and the error appears at the same SoC level. Such results may support the conclusion mentioned in the last section that the negative electrode dominantly contributes to the low-SoC-area error.

In addition, the goodness-of-fit (R^2), voltage RMSE, and maximum error under the discharge and charge profiles are compared and then listed in Table 4. According to the R^2 results, although the NLECM-diff model has a slightly worse accuracy, the difference between NLECM-diff and SPMe are minor in the 0.3C (0.78%) and 0.5C (0.79%) cases, however, there is a 2.74% reduction than SPMe in accuracy of the NLECM-diff model during the 1C discharge. Likewise, the RMSE and maximum error results report that the NLECM-diff model has larger voltage error than

SPMe in the long time discharge and charge tests. Furthermore, Table 4 presents computational time of two models using the same PC hardware with the CPU of Intel Core i7 and 16.0GB RAM for simulating the 1C discharge working condition, and the result indicates that the computational cost of the NLECM-diff model is substantially lower than the SPMe model.

Table 4
Accuracy and computational time comparison of SPMe and NLECM-diff in long time discharge and charge tests.

	Goodness-of-fit (R^2) [%]			RMSE [V]			Maximum Error [V]			Computational Time [s]
	0.3C	0.5C	1C	0.3C	0.5C	1C	0.3C	0.5C	1C	1C
SPMe	99.48	99.56	97.05	0.037	0.035	0.062	0.157	0.107	0.514	270.76
NLECM-diff	98.70	98.77	94.31	0.058	0.054	0.087	0.219	0.117	0.531	3.93

Overall, by comparing the estimated voltage and error, it is shown that the model estimation error increases as the excitation current enhances and the SoC decreases. Furthermore, the accuracy of the NLECM-diff model is slightly lower than the SPMe under CC discharge and CC-CV charge profiles.

4.3. Results under NEDC profile - Full Cell

A further model validation is carried out under the New European Driving Cycle (NEDC) load profile. The NEDC is a typical dynamic experiment cycle to test the performance of light-duty vehicle models in the European Union, which consists of periods of constant acceleration, deceleration and speed [58]. As shown in Fig.9(a), the test is performed starting from fully charged until the terminal voltage reaches the cut-off voltage 2.5 V. The zoom-in figure corresponds to the current with average SoC in the 10th cycle, where the SoC changes from 55.9% to 51.3% in a NEDC cycle within 0.33 h. In addition, the estimated voltage of the SPMe and the NLECM-diff model are compared with the measured voltage under the NEDC test as well as the detailed 10th cycle results in Fig.9(b). A total of nineteen complete plus a partial NEDC cycles are accomplished in this test, and the 10th and 19th cycles are analysed in detail. According to the zoom-in figure in Fig.9(b), the NLECM-diff model can capture the cell voltage response and has a good agreement with the SPMe, however, the voltage amplitude estimated by the NLECM-diff model is smaller than the SPMe at peak values. Note that, in the end of the NEDC test, the model voltage value, which is less than 2.5 V, is the limitation of mathematical models caused by the extrapolation, which requires to set saturation to avoid.

Fig.9(c) illustrates the voltage error in the 10th cycle with the black dashed lines as the ±0.05 V boundaries. Most of the voltage error is within the ±0.05 V range, but an underestimation is noticed for the estimated voltage in the NEDC cycle. Fig.9(d) is related to the 19th cycle in low SoC range with SoC 13.6% − 8.9%. Compared with the results in the 10th cycle, a obvious underestimation, which is out of the boundaries, can be noticed and the largest error appears at the end of each NEDC cycle caused by 22 mA (about 2C) current discharge. Furthermore, the NLECM-diff model shows a better performance (smaller error) than the SPMe in this cycle.

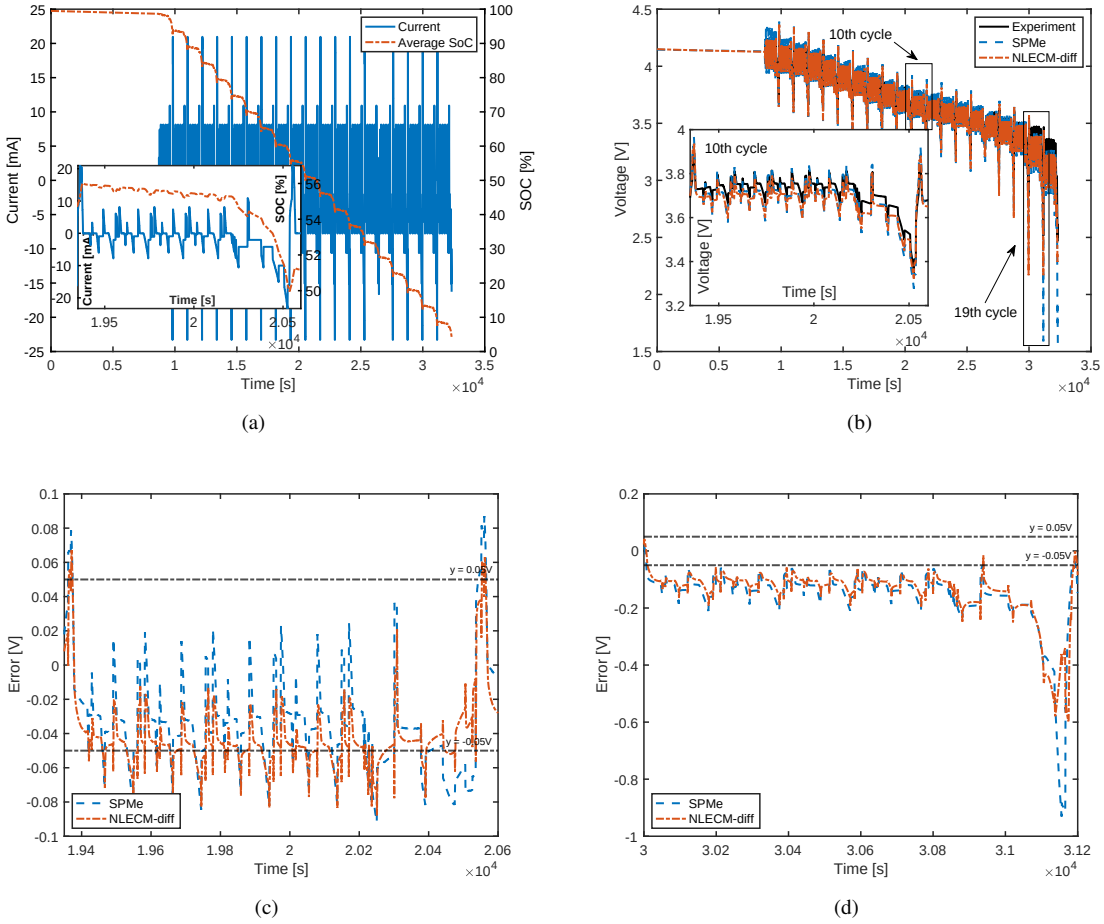

Fig. 9. Comparison of SPMe and NLECM-diff in NEDC test: (a) Current and SoC variation; (b) Voltage estimation results; (c) Voltage Error in the 10th cycle; (d) Voltage Error in the 19th cycle.

The accuracy and computational time of models under the NEDC test are compared and then listed in Table 5. The goodness-of-fit R^2 results illustrate that the NLECM-diff model has 2.78% higher accuracy than the SPMe in the NEDC dynamic profile. According to the RMSE voltage results, the NLECM-diff model shows a 0.11 V RMSE higher accuracy than the SPMe. The maximum error is observed in the two models when the SoC reaches low stage (close to 0%). Such error is likely from the error of negative electrode OCV measurement, which requires further investigation in the future work. Additionally, similar to computational cost results presented in Section 4.2, Table 5 indicates that the NLECM-diff model has a significantly lower computational burden than the SPMe model.

In this section, the NEDC driving cycle test is carried out for validation and the estimated voltage of two models are compared. The results show that the estimated voltage error increases as the SoC decreases, which is consistent with the results in previous sections. Additionally, the accuracy of the NLECM-diff model is demonstrated to be superior to that of the SPMe, which indicates the NLECM-diff model may be more suitable for use during the dynamic driving

Table 5
Accuracy and computational time comparison of SPMe and NLECM-diff in NEDC test.

	Goodness-of-fit (R^2) [%]	RMSE [V]	Maximum Error [V]	Computational Time [s]
SPMe	92.83	0.085	0.930	514.75
NLECM-diff	95.61	0.074	0.780	6.02

cycle.

4.4. Dominant electrochemical process under different load profiles

In this section, the fundamental rationale, which leads to the higher accuracy of the NLECM-diff model in the NEDC test rather than in the 1C constant current discharge, is discussed according to the variation of surface SoC and average SoC obtained by the diffusion block. Furthermore, the dominant electrochemical process in a lithium-ion battery under different profiles is determined by analysing voltage losses of the NLECM-diff model.

Fig.10(a) and Fig.10(b) show the comparison between the surface SoC and average SoC under the 1C constant current discharge and the NEDC profile, respectively. It's clear to observe that the difference between surface SoC and average SoC appears in these tests when the excitation starts and the battery equilibrium state no longer exists. In Fig.10(a), the surface SoC is always less than the average SoC at the same moment during the discharge. According to the purple line, which indicates the difference between the surface SoC and average SoC, termed as ΔSoC, it's shown that the absolute value of ΔSoC gradually increases from 0 to the maximum value of 22.8% when the battery is discharged to 64% average SoC, and maintains the maximum value until the discharge ends, then gradually decreases to 0 through the relaxation process. Recall the estimated voltage results in Fig.8(c), it is reported that the start of the deviation of estimated voltage also appears at 64% average SoC, and when the measured voltage reaches the cut-off voltage, the remaining 22.8% SoC is exactly same as the maximum difference between the surface SoC and average SoC. Such results illustrate a strong dependence between the large estimated voltage error at 1C discharge and the SoC difference ΔSoC caused by the diffusion process. As described in Section 3.5, Q and τ_d are two parameters which requires to be identified in the diffusion block. In Fig.8(c), when the battery relaxes to the equilibrium state after 1C discharge, the estimated voltage of the NLECM-diff model is overlapped on the measured experimental voltage data, which indicates the released capacity estimated by the NLECM-diff model is identical to the actual extracted capacity from the cell in the test, thus it can be confirmed that the parameter Q, which is related to the cell capacity, is accurately identified. On the other side, because the NLECM-diff model is optimised at 0.5C, the significant voltage error observed during discharging could be caused by the fact that the variation of the diffusion-related characteristics results in the identified diffusion-related time constant τ_d is inappropriate for the case of the 1C discharge. Taking into account that the voltage error and the maximum ΔSoC concurrently appear, the reason may be attributed to the value of τ_d in adequately simulating the greater ΔSoC caused by the diffusion process under large current loads. Note that, as described in Section 4.1, the negative electrode is determined as the origin of the low-SoC-area error, the dominant

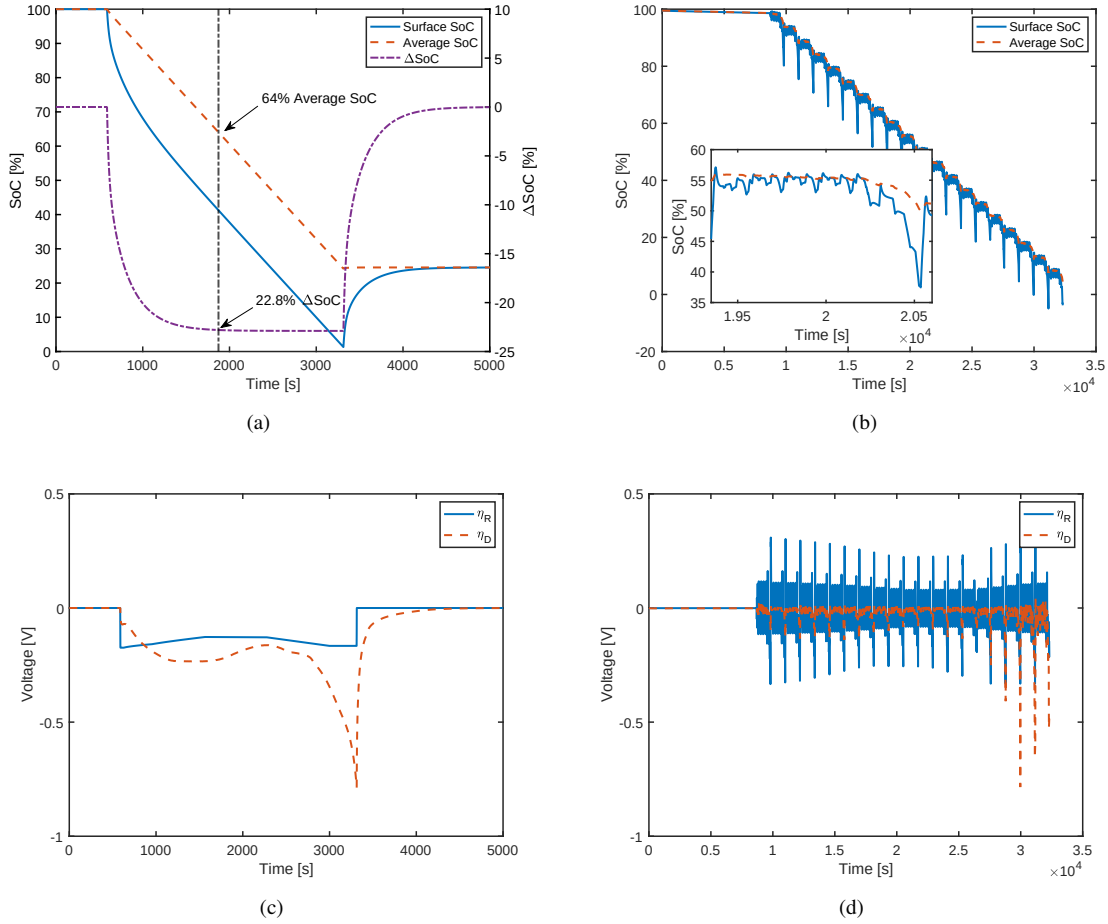

Fig. 10. Comparison between SoCs and between voltage losses under different load profiles: (a) Comparison between surface SoC and average SoC under 1C discharge; (b) Comparison between surface SoC and average SoC under NEDC profile; (c) Comparison between ohmic and diffusion process voltage loss under 1C discharge; (d) Comparison between ohmic and diffusion process voltage loss under NEDC profile.

factor is thus determined as the diffusion-related characteristic changes of the negative electrode, which leads to the considerable error in the low SoC region under high current load. In addition, Fig.10(b) reports the variation of the surface SoC and average SoC in the NEDC test and the 10th cycle shown in detailed. It's demonstrated that the variation of surface SoC is more drastic than average SoC in the whole test, and the maximum 12.4% SoC difference is found within a single NEDC cycle. Given that the maximum SoC difference that the NLECM-diff model parameterised at 0.5C discharge case can provide is 22.8% greater than 12.4%, the diffusion block with the identified parameter τ_d is sufficient to provide the dynamic response caused by diffusion processes, which may be the reason that the NLECM-diff shows high accuracy under the strong dynamic NEDC profile.

In order to understand the role of electrochemical processes inside a lithium-ion battery, the dominant battery losses under different current loads is determined using the NLECM-diff model. Fig.10(c) and Fig.10(d) exhibit the

variation of the ohmic voltage loss with charge-transfer reaction effect η_R and the voltage loss caused by diffusion process η_D under different load profiles. During the 1C constant current discharge, it's noticed that both η_R and η_D exist when the discharge starts. The η_R is shown as the dominant voltage loss contributor at the beginning, then, as the discharge duration increases, the η_D replaces η_R to contribute most voltage loss in the estimated voltage output. At the end of discharge process, the voltage loss contributed by the η_D is 4.93 times than that by the η_R. Contrary to the constant current discharge, it's obviously shown that the η_R is the dominant voltage loss contributor in most of the NEDC test in Fig.10(d), except for several peak current moments within the low SoC range. It can therefore be concluded that the diffusion process is the behaviour dominating the battery voltage under the large current load profile, but in the strong dynamic load profile, e.g. NEDC, the ohmic voltage loss with charge-transfer reaction effect becomes to the dominant contributor.

5. Conclusion and future work

This paper presents a non-linear equivalent circuit model with diffusion dynamics, termed as a NLECM-diff, which is identified with a multisine-based nonlinear characterisation method and a constant current discharge method. The NLECM-diff model is able to account for the battery electrochemical processes, in which a 2nd order linear equivalent circuit model (ECM) presents the battery impedance, a sigmoid function accounts for any non-linearity, and a lumped SoC dependent diffusion block accounts for the solid-phase diffusion process. Furthermore, the surface SoC and average SoC are calculated by the proposed model, thus the diffusion process voltage loss and the open circuit potential can be determined correspondingly. Taking advantage of the three-electrode cell used in this work, not only the NLECM-diff model for a full cell but also for individual electrodes are developed. The accuracy of the NLECM-diff models is validated in two types current load experiments as well as compared with the widely-used single particle model with electrolyte dynamics (SPMe).

In this paper, the conclusions are listed as follow:

(i) By introducing the diffusion block at the cost of adding two extra identifiable parameters, the voltage estimation error in the low SoC range is significantly reduced by the NLECM-diff model and the RMSE value decreases by more than 49.6% in comparison of the conventional NLECM.

(ii) In comparison to the SPMe which necessitates extensive experimental characterisation for a total of 29 parameters, the NLECM-diff model requires only 10 easily-identifiable parameters, as listed in Table 1, but can achieve comparable accuracy with the electrochemical model. In addition, as the computational cost is low (See Table 4 and 5), the NLECM-diff model is a suitable candidate for accurate voltage estimation in BMS applications.

(iii) The dominant behaviour contributing to the voltage loss is determined by using the NLECM-diff model in different current load cases, in which the diffusion process is the dominant voltage loss when under the long

time current discharge and the ohmic voltage loss is the dominant dynamic when under a dynamic NEDC profile.

(iv) The de-coupled electrode NLECM-diff models are established for the three-electrode cell using the potential data of positive and negative electrodes measured in the same identification tests. The validation results suggest that, during discharging, the larger estimated error of the positive electrode NLECM-diff model is observed in the middle SoC range, whereas the negative electrode NLECM-diff model has a considerable voltage error in the low SoC region. In addition, by comparing with the SPMe electrodes response under the identical current load, the variation of the diffusion-related characteristics of the negative electrode is determined as the primary reason of the battery models' large low-SoC-area error under different current intensities.

The future work will focus on the SoC estimation method design based on the NLECM-diff model, as well as the model identification and performance evaluation at various working conditions, such as temperature, SOC intervals and discharging rates, especially at the low temperature when the strong nonlinearity appears.

Acknowledgement

The research presented within this paper was supported by WMG, University of Warwick (09ESWM21), Institute of Digital Engineering (IDE) under a grant for Virtually Connected Hybrid Vehicle project, and The Faraday Institution "Multi-Scale Modelling" project [EP/S003053/1 grant number FIRG003]."

Appendix A. Discrete Chebyshev-Gauss-Lobatto orthogonal collocation method

Refer to [55], in the orthogonal collocation method, the grid points are defined by

$$y_j = \cos\frac{j\pi}{N}, \qquad j = 0, ..., N \tag{A.1}$$

where j is the index of grid points. Mathematically, y_j represents the locations of the extrema of the first kind Chebyshev polynomials, $T_N(l) = \cos(N \arccos(l))$. The $(N+1) \times (N+1)$ Chebyshev derivative matrix D at the quadrature points is:

$$D = (d_{jk})_{0 \le j \le N, 0 \le k \le N} \tag{A.2}$$

with

$$\begin{cases} d_{00} = \dfrac{2N^2+1}{6} \\ d_{jj} = -\dfrac{x_j}{2(1-y_j^2)} \qquad 1 \le j \le N-1 \\ d_{NN} = -\dfrac{2N^2+1}{6} \end{cases}$$

For $0 \le j \le N, 0 \le k \le N$ with $j \ne k$, the element d_{jk} is

$$d_{jk} = \frac{c_j(-1)^{j+k}}{c_k(y_j - y_k)}$$

with

$$\begin{cases} c_0 = 2 \\ c_j = 1 \qquad 1 \le j \le N-1 \\ c_k = 1 \qquad 1 \le k \le N-1 \\ c_N = 2 \end{cases}$$

If v is the vector formed by the values of the function $u(y)$ at the locations $y_j, j = 0, ..., N$, the values of the approximations v' and v'' of the derivates u' and u'' of u at the grid points y_j are calculated as follows:

$$v' = Dv; \qquad v'' = D^2 v$$

where D is the differentiation matrix. .

References

[1] R. Xiong, Y. Pan, W. Shen, H. Li, F. Sun, Lithium-ion battery aging mechanisms and diagnosis method for automotive applications: Recent advances and perspectives, Renewable and Sustainable Energy Reviews 131 (2020) 110048.

[2] X. Hu, H. Yuan, C. Zou, Z. Li, L. Zhang, Co-estimation of state of charge and state of health for lithium-ion batteries based on fractional-order calculus, IEEE Transactions on Vehicular Technology 67 (11) (2018) 10319–10329.

[3] Y. Zhang, R. Xiong, H. He, X. Qu, M. Pecht, State of charge-dependent aging mechanisms in graphite/li (nicoal) o2 cells: Capacity loss modeling and remaining useful life prediction, Applied Energy 255 (2019) 113818.

[4] C. She, L. Zhang, Z. Wang, F. Sun, P. Liu, C. Song, Battery state of health estimation based on incremental capacity analysis method: synthesizing from cell-level test to real-world application, IEEE Journal of Emerging and Selected Topics in Power Electronics.

[5] K. Liu, K. Li, C. Zhang, Constrained generalized predictive control of battery charging process based on a coupled thermoelectric model, Journal of Power Sources 347 (2017) 145–158.

[6] J. Sun, Q. Ma, C. Tang, T. Wang, T. Jiang, Y. Tang, Research on optimization of charging strategy control for aged batteries, IEEE Transactions on Vehicular Technology.

[7] Z. Wang, C. Song, L. Zhang, Y. Zhao, P. Liu, D. G. Dorrell, A data-driven method for battery charging capacity abnormality diagnosis in electric vehicle applications, IEEE Transactions on Transportation Electrification.

[8] S. Jinlei, L. Wei, T. Chuanyu, W. Tianru, J. Tao, T. Yong, A novel active equalization method for series-connected battery packs based on clustering analysis with genetic algorithm, IEEE Transactions on Power Electronics 36 (7) (2021) 7853–7865.

[9] K. Liu, X. Hu, Z. Yang, Y. Xie, S. Feng, Lithium-ion battery charging management considering economic costs of electrical energy loss and battery degradation, Energy conversion and management 195 (2019) 167–179.

[10] M. Doyle, T. F. Fuller, J. Newman, Modeling of galvanostatic charge and discharge of the lithium/polymer/insertion cell, Journal of the Electrochemical society 140 (6) (1993) 1526.

[11] G. Ning, B. N. Popov, Cycle life modeling of lithium-ion batteries, Journal of The Electrochemical Society 151 (10) (2004) A1584.

[12] X. G. Yang, Y. Leng, G. Zhang, S. Ge, C. Y. Wang, Modeling of lithium plating induced aging of lithium-ion batteries: Transition from linear to nonlinear aging, Journal of Power Sources 360 (2017) 28–40. doi:10.1016/j.jpowsour.2017.05.110.
URL http://dx.doi.org/10.1016/j.jpowsour.2017.05.110

[13] C.-H. Chen, F. Brosa Planella, K. O'Regan, D. Gastol, W. D. Widanage, E. Kendrick, Development of Experimental Techniques for Parameterization of Multi-scale Lithium-ion Battery Models, Journal of The Electrochemical Society 167 (8) (2020) 080534. doi:10.1149/1945-7111/ab9050.

[14] S. Santhanagopalan, Q. Guo, P. Ramadass, R. E. White, Review of models for predicting the cycling performance of lithium ion batteries, Journal of power sources 156 (2) (2006) 620–628.

[15] S. J. Moura, F. B. Argomedo, R. Klein, A. Mirtabatabaei, M. Krstic, Battery state estimation for a single particle model with electrolyte dynamics, IEEE Transactions on Control Systems Technology 25 (2) (2016) 453–468.

[16] C. Fan, M. D. Higgins, W. D. Widanage, Real-time state of charge estimation of electrochemical model for lithium-ion battery, in: 2019 IEEE Vehicle Power and Propulsion Conference (VPPC), IEEE, 2019, pp. 1–6.

[17] K. A. Smith, C. D. Rahn, C.-Y. Wang, Model order reduction of 1d diffusion systems via residue grouping, Journal of Dynamic Systems, Measurement, and Control 130 (1).

[18] L. Li, Y. Ren, K. O'Regan, U. R. Koleti, E. Kendrick, W. D. Widanage, J. Marco, Lithium-ion battery cathode and anode potential observer based on reduced-order electrochemical single particle model, Journal of Energy Storage 44 (2021) 103324.

[19] M. Jun, K. Smith, P. Graf, State-space representation of li-ion battery porous electrode impedance model with balanced model reduction, Journal of Power Sources 273 (2015) 1226–1236.

[20] J. C. Forman, S. Bashash, J. L. Stein, H. K. Fathy, Reduction of an electrochemistry-based li-ion battery model via quasi-linearization and pade approximation, Journal of the Electrochemical Society 158 (2) (2010) A93.

[21] X. Hu, S. Li, H. Peng, A comparative study of equivalent circuit models for Li-ion batteries, Journal of Power Sources 198 (2012) 359–367. doi:10.1016/j.jpowsour.2011.10.013.

[22] M. Bruch, L. Millet, J. Kowal, M. Vetter, Novel method for the parameterization of a reliable equivalent circuit model for the precise simulation of a battery cell's electric behavior, Journal of Power Sources 490 (2021) 229513.

[23] A. Hentunen, T. Lehmuspelto, J. Suomela, Time-domain parameter extraction method for thévenin-equivalent circuit battery models, ieee transactions on energy conversion 29 (3) (2014) 558–566.

[24] W. D. Widanage, A. Barai, G. H. Chouchelamane, K. Uddin, A. McGordon, J. Marco, P. Jennings, Design and use of multisine signals for Li-ion battery equivalent circuit modelling. Part 2: Model estimation, Journal of Power Sources 324 (2016) 61–69. doi:10.1016/j.jpowsour.2016.05.014.

[25] R. Relan, Y. Firouz, J.-M. Timmermans, J. Schoukens, Data-driven nonlinear identification of li-ion battery based on a frequency domain nonparametric analysis, IEEE Transactions on Control Systems Technology 25 (5) (2016) 1825–1832.

[26] G. L. Plett, Extended Kalman filtering for battery management systems of LiPB-based HEV battery packs - Part 1. Background, Journal of Power Sources 134 (2) (2004) 252–261. doi:10.1016/j.jpowsour.2004.02.031.

[27] G. L. Plett, Extended kalman filtering for battery management systems of lipb-based hev battery packs: Part 2. modeling and identification, Journal of power sources 134 (2) (2004) 262–276.

[28] G. L. Plett, Extended kalman filtering for battery management systems of lipb-based hev battery packs: Part 3. state and parameter estimation, Journal of Power sources 134 (2) (2004) 277–292.

[29] W. D. Widanage, A. Barai, G. H. Chouchelamane, K. Uddin, A. McGordon, J. Marco, P. Jennings, Design and use of multisine signals for Li-ion battery equivalent circuit modelling. Part 1: Signal design, Journal of Power Sources 324 (2016) 70–78. doi:10.1016/j.jpowsour.2016.05.015.

[30] Y. Firouz, S. Goutam, M. C. Soult, A. Mohammadi, J. Van Mierlo, P. Van den Bossche, Block-oriented system identification for nonlinear modeling of all-solid-state li-ion battery technology, Journal of Energy Storage 28 (2020) 101184.

[31] W. Allafi, K. Uddin, C. Zhang, R. M. R. A. Sha, J. Marco, On-line scheme for parameter estimation of nonlinear lithium ion battery equivalent circuit models using the simplified refined instrumental variable method for a modified wiener continuous-time model, Applied energy 204 (2017) 497–508.

[32] S. Wang, M. Verbrugge, J. S. Wang, P. Liu, Power prediction from a battery state estimator that incorporates diffusion resistance, Journal of Power Sources 214 (2012) 399–406.

[33] M. Ouyang, G. Liu, L. Lu, J. Li, X. Han, Enhancing the estimation accuracy in low state-of-charge area: A novel onboard battery model through surface state of charge determination, Journal of Power Sources 270 (2014) 221–237.

[34] H. Ekström, B. Fridholm, G. Lindbergh, Comparison of lumped diffusion models for voltage prediction of a lithium-ion battery cell during dynamic loads, Journal of Power Sources 402 (2018) 296–300.

[35] D. Guo, G. Yang, X. Feng, X. Han, L. Lu, M. Ouyang, Physics-based fractional-order model with simplified solid phase diffusion of lithium-ion battery, Journal of Energy Storage 30 (2020) 101404.

[36] C. Fan, K. O'Regan, L. Li, E. Kendrick, W. Widanage, Frequency domain non-linear characterization and analysis of lithium-ion battery electrodes, Journal of Energy Storage 36 (2021) 102371.

[37] Y. Firouz, R. Relan, J. Timmermans, N. Omar, P. Van Den Bossche, J. Van Mierlo, Advanced lithium ion battery modeling and nonlinear analysis based on robust method in frequency domain: Nonlinear characterization and non-parametric modeling, Energy 106 (2016) 602–617.

[38] J. Schoukens, R. Pintelon, Y. Rolain, Mastering system identification in 100 exercises, John Wiley & Sons, 2012.

[39] E. Evans, D. Rees, L. Jones, Nonlinear disturbance errors in system identification using multisine test signals, IEEE Transactions on Instrumentation and Measurement 43 (2) (1994) 238–244.

[40] C. Fan, T. R. Grandjean, K. O'Regan, E. Kendrick, W. D. Widanage, Understanding non-linearity in electrochemical systems using multisine-based non-linear characterization, Transactions of the Institute of Measurement and Control (2021) 01423312211045991.

[41] W. D. Widanage, J. Stoev, J. Schoukens, Design and application of signals for nonlinear system identification, IFAC Proceedings Volumes

45 (16) (2012) 1605–1610.

[42] J. Schoukens, T. Dobrowiecki, Design of broadband excitation signals with a user imposed power spectrum and amplitude distribution, in: IMTC/98 Conference Proceedings. IEEE Instrumentation and Measurement Technology Conference. Where Instrumentation is Going (Cat. No. 98CH36222), Vol. 2, IEEE, 1998, pp. 1002–1005.

[43] R. Pintelon, J. Schoukens, System Identification: A Frequency Domain Approach, Second Edition, John Wiley and Sons, 2012. doi:10.1002/9781118287422.

[44] R. Pintelon, J. Schoukens, G. Vandersteen, K. Barbé, Estimation of nonparametric noise and frf models for multivariable systems—part i: Theory, Mechanical Systems and Signal Processing 24 (3) (2010) 573–595.

[45] I. Kollár, R. Pintelon, J. Schoukens, Frequency domain system identification toolbox for matlab, IFAC Proceedings Volumes 24 (3) (1991) 1243–1247.

[46] A. Jossen, Fundamentals of battery dynamics, Journal of power sources 154 (2) (2006) 530–538.

[47] N. Wolff, N. Harting, F. Röder, M. Heinrich, U. Krewer, Understanding nonlinearity in electrochemical systems, The European Physical Journal Special Topics 227 (18) (2019) 2617–2640.

[48] B. Pattipati, B. Balasingam, G. Avvari, K. Pattipati, Y. Bar-Shalom, Open circuit voltage characterization of lithium-ion batteries, Journal of Power Sources 269 (2014) 317–333.

[49] J. Newman, K. E. Thomas-Alyea, Electrochemical systems, John Wiley & Sons, 2012.

[50] J. Li, J. K. Barillas, C. Guenther, M. A. Danzer, A comparative study of state of charge estimation algorithms for lifepo4 batteries used in electric vehicles, Journal of power sources 230 (2013) 244–250.

[51] G. I. El-Baghdady, M. El-Azab, Chebyshev-gauss-lobatto pseudo-spectral method for one-dimensional advection-diffusion equation with variable coefficients, Math 3 (1) (2016) 1–8.

[52] D. Di Domenico, A. Stefanopoulou, G. Fiengo, Lithium-ion battery state of charge and critical surface charge estimation using an electrochemical model-based extended kalman filter, Journal of dynamic systems, measurement, and control 132 (6).

[53] C. D. Rahn, C.-Y. Wang, Battery systems engineering, John Wiley & Sons, 2013.

[54] B. Fornberg, The pseudospectral method: Comparisons with finite differences for the elastic wave equation, Geophysics 52 (4) (1987) 483–501.

[55] H. Binous, A. A. Shaikh, A. Bellagi, Chebyshev orthogonal collocation technique to solve transport phenomena problems with matlab® and mathematica, Computer Applications in Engineering Education 23 (3) (2015) 422–431.

[56] S. Kirkpatrick, C. D. Gelatt, M. P. Vecchi, Optimization by simulated annealing, science 220 (4598) (1983) 671–680.

[57] C. Liu, Y. Gao, L. Liu, Toward safe and rapid battery charging: Design optimal fast charging strategies thorough a physics-based model considering lithium plating, International Journal of Energy Research 45 (2) (2021) 2303–2320.

[58] T. J. BARLOW, S. Latham, I. McCrae, P. Boulter, A reference book of driving cycles for use in the measurement of road vehicle emissions, TRL Published Project Report.